An efficient and generalisable approach for mapping paddy rice fields based on their unique spectra during the transplanting period leveraging the CIE colour space

Huapeng Li [a, b *], Jujian Huang [a, c], Ce Zhang [d, e], Xiangyu Ning [a, f], Shuqing Zhang [a, b], Peter M. Atkinson [g, h]

[a] State Key Laboratory of Black Soils Conservation and Utilization, Northeast Institute of Geography and Agroecology, Chinese Academy of Sciences, Changchun 130102, China; [b] Jilin Provincial Key Laboratory of Remotely Sensed Big Data for Ecology and Environment Research, Changchun 130102, China; [c] School of Geomatics and Prospecting Engineering, Jilin Jianzhu University, Changchun 130118, China; [d] School of Geographical Sciences, University of Bristol, Bristol BS8 1SS, UK; [e] UK Centre for Ecology & Hydrology, Library Avenue, Bailrigg, Lancaster LA1 4AP, UK; [f] University of Chinese Academy of Sciences, Beijing 100049, China; [g] Faculty of Science and Technology, Lancaster University, Lancaster, LA1 4YR, UK; [h] Geography and Environmental Science, University of Southampton, Highfield, Southampton SO17 1BJ, UK

Abstract As one of the most important staple foods globally, rice sustains nearly half of the world's population. Accurate and timely paddy rice mapping is, thus, essential for rice-related policy-making to ensure food security in the context of anthropogenic, environmental and climate changes. However, paddy rice mapping remains a challenging task since it usually has similar spectral characteristics to other land covers. In this research, for the first time, an entirely new approach, called RiceTColour, was proposed for mapping rice fields within the Commission Internationale de l'Eclairage (CIE) colour space based on their unique spectra during the rice transplanting period as observed in remotely sensed imagery. We demonstrate that transplanted rice fields, representing a mixture of soil, water and rice seedlings, consistently exhibit relatively low spectral values in both SWIR and NIR bands across various geographical locations, leading to their unique dark green colours in the false-colour image composed of SWIR, NIR and Red bands. Based upon this, we transformed these three spectral bands into the CIE colour space where paddy rice was found to be readily and completely separated from the other land covers. Straightforward, but specific classification criteria were established within the CIE colour space to differentiate paddy rice from the other land covers. The proposed RiceTColour, thus, represents a new approach for paddy rice identification, that is mapping paddy rice using the CIE colour space based upon the previous underexplored remotely sensed spectra of paddy fields during the transplanting season. The effectiveness of the proposed method was investigated over five rice-planting regions distributed across different geographical regions, characterised by different climates, rice cropping intensities, irrigation schemes and cultural practices. Specifically, the mapping criteria established in a training site (S1) were directly generalised to the other four sites (S2 to S5) for paddy rice mapping. Experimental results demonstrated that the RiceTColour method consistently achieved the most accurate and balanced classifications across all five sites compared with four benchmark comparators: a SAR-based method, an index-based method and two supervised classifier-based methods. In particular, the RiceTColour method performed relatively stable, producing an overall accuracy exceeding 95% in the training site (S1) as well as the four generalised sites (S2 to S5), which is an encouraging result. Such efficient yet stable rice mapping results across various rice-planting regions suggest a very strong generalisation capability of the proposed RiceTColour method. In consideration of the relatively large planting area of paddy rice fields globally, the proposed parameter-free, efficient, and generalisable RiceTColour method, thus, holds great potential for widespread application in various rice-planting areas worldwide.

Keywords: paddy rice; rice mapping; classification method; transplanting period; colours of rice fields

1. Introduction

Paddy rice, a common staple food, feeds nearly half of the world's population while occupying only 12% of the global cropland area (Bouman, 2009; FAO, 2022). The global production of paddy rice in 2020 was about 757 million tonnes, accounting for more than 8% of the world's total grain production (FAO, 2022). As the only major crop planted and grown in flooded soil (Xu et al., 2023), paddy rice consumes more water than other crops at the field level; roughly one quarter to one-third of the Earth's accessible freshwater reserves are designated for irrigating paddy rice fields (Bouman, 2009). Moreover, as a major source of CH_4 emissions, paddy rice accounted for approximately 8% of the total anthropogenically-induced global methane emissions from 2008 to 2017 (Saunois et al., 2020). As a result, accurate and timely mapping of paddy rice is not only fundamentally important to ensure global food security, but also essential for studying environment-related issues, such as climate change and water resource management.

Compared with traditional field surveys, satellite remote sensing has demonstrated distinctive advantages in terms of paddy rice mapping and monitoring, including large area coverage, timely monitoring, and low cost (Xiao et al., 2005; Qin et al., 2015; Kontgis et al., 2015; Han et al., 2022). Besides, remote sensing-based rice mapping is relatively objective and less influenced by human experience. Historical time-series images of paddy rice are, therefore, comparable from regional-to-national scales, which is especially beneficial for accurately identifying expanding or shrinking areas of paddy rice (Kontgis et al., 2015; Dong et al., 2016; Carrasco et al., 2022; Han et al., 2022).

Previous research has illustrated that rice-planting areas can be characterised during the early growing season using remote sensing (Stroppiana et al., 2019; Zhan et al., 2021), which provides strong support for decision-making amongst governments and farmers regarding rice planting and marketing. Since the launch of Landsat-1 in 1972, satellite remotely sensed images have been employed widely for paddy rice mapping and monitoring using a variety of classification and mapping methods (McCloy et al., 1987; LeToan et al., 1997; Xiao et al., 2005; Dong et al., 2016; Ni et al., 2021; Xu et al., 2023), which can be generally categorised into three types: classifier-based, phenology-based and index-based methods.

Classifier-based methods are the most commonly-used for rice mapping, especially supervised classifiers which depend on training samples (Dong and Xiao, 2016). The maximum likelihood classifier (MLC) was adopted widely in the 1980s and 1990s (e.g., McCloy et al., 1987; Panigrahy and Parihar, 1992), but the accuracy of this parametric classifier is largely dependent on the representativeness of the Gaussian model of the data distribution (Lu and Weng, 2007). Benefiting from the rapid development in computer science and artificial intelligence technologies, machine learning (ML) algorithms, such as random forests (RFs), artificial neural networks (ANNs) and support vector machines (SVMs), which are independent of the data distribution, have gradually evolved as mainstream classifiers (Shao et al., 2001; Chen and McNairn, 2006; Onojeghuo et al., 2018; Ni et al., 2021). However, these data-driven classifiers, typically consisting of one or two shallow layers, are unable to extract deep features from remotely sensed imagery to aid the classification (Chen et al., 2015). Recently, deep learning, a novel variant of ML, has garnered increasing interest in the field of image classification owing to its capability of obtaining deep feature representations (Krizhevsky et al., 2012; LeCun et al., 2015). Although these ML classifiers have been employed widely in rice mapping applications, both shallow and deep-structured classifiers typically encounter two critical issues. First, their high accuracy often relies heavily on acquiring a large-volume of high-quality samples, which can be challenging to achieve in practice, especially over expansive regions (Nogueira et al., 2017). Second, these are essentially local optimal models established based on specific samples. Consequently, these classifiers, along with their optimised hyperparameters, are very challenging to generalise to unseen data (Zhang et al., 2020).

Phenology-based approaches differentiate paddy rice from other land covers by analysing the temporal variation in vegetation indices, such as the Land Surface Water Index (LSWI), Normalized Difference Vegetation Index (NDVI) and Enhanced Vegetation Index (EVI), throughout the full year (growing season) time-series (Xiao et al., 2002; Xiao et al., 2005). Phenology-based methods typically adopt a set of classification rules expressed in the form of decision trees, in which one or more thresholds need to be determined. The primary hypothesis behind such methods is that paddy rice is the sole crop cultivated in flooded soil, consequently possessing distinctive physical characteristics and displaying specific signals, such as higher water content, in the time-series of vegetation indices during the early growing season (flooding and transplanting periods). Using optical remotely sensed imagery, Xiao et al. (2002) was the first to discover that the LSWI (water content indicator) temporally exceeds the NDVI (EVI) (vegetation greenness indicator) during the unique flooding and transplanting periods of paddy rice. Based on this unique signal, Xiao et al. (2005) proposed a simple yet effective phenology- and pixel-based paddy rice mapping (PPPM) method using MODIS time-series. Since then, this method has gained increasing attention within the crop mapping community, and several variants have been developed for rice mapping in a range of rice-planting areas (Xiao et al., 2006; Sakamoto et al., 2009; Peng et al., 2011; Kontgis et al., 2015; Dong et al., 2015; Dong et al., 2016; Maiti et al., 2022). Phenology-based methods, based on the unique and stable physical features of paddy rice, do not rely on training samples and consequently tend to perform more robustly than classifier-based methods (Rad et al., 2019; Tian et al., 2023; Zhang et al., 2023). However, they usually require a full year (growing season) time-series to detect paddy rice and build masks of other land covers, which not only consumes a significant amount of time and effort in preparation, but can also be difficult to attain in real applications due to cloud contamination, especially for satellites with long revisit cycles, such as the Landsat satellite series. As such, most of the previous studies selected daily-acquired MODIS imagery as the data source for rice mapping (Xiao et al., 2006; Peng et al., 2011; Bridhikitti and Overcampb, 2012; Zhang et al., 2015; Luintel et al., 2021). Furthermore, it can be challenging to generalise these methods to large new regions with fixed thresholds in consideration of the great variabilities of paddy rice caused by climatic conditions, rice variety and farmers' management practices (Le Toan et al., 1997; Dong et al., 2016).

Index-based methods combining several spectral bands at different wavelengths to highlight the difference between the target class and other classes have been employed widely for crop mapping and monitoring (Ashourloo et al., 2019; Xu et al., 2023). They have apparent advantages over phenology-based methods in their simplicity and low computational cost (e.g., Chen et al., 2023). Boschetti et al. (2014) evaluated extensively the capability of various Normalised Difference Spectral Indices for the detection of flooded rice fields using MODIS imagery, and the Normalized Difference Water Index (NDWI) was found to perform most accurately amongst the indices. Recently, Xu et al. (2023) proposed a SAR-based Paddy Rice Index (SPRI) to map paddy rice using Sentinel-1 time-series collected during the transplanting-vegetative period. However, few studies have developed specific vegetation indices for paddy rice mapping from optical remotely sensed imagery. Besides, similar to phenology-based methods, determining universal thresholds for accurate rice mapping over different rice-planting areas is generally very challenging due to the high temporal and spatial variability across rice fields (Le Toan et al., 1997; Dong et al., 2016).

Although the above-mentioned developments in methods have made great contributions to paddy rice mapping and have yielded promising results in specific regions, there remain three main challenges to progress: (1) they are hard to generalise to new rice-planting areas; (2) there exist difficulties in determining the optimal hyperparameters or thresholds; and (3) they usually rely on full year (growing season) image time-series. In fact, despite variations in climate conditions and cultural practices, paddy rice fields have similar physical features during the transplanting period across different regions, characterised by a mixture of soil, water and vegetation. Consequently, they should consistently present unique and stable spectra, along with distinct colours in remote sensed imagery when an appropriate combination of spectral bands is adopted. This suggests potential opportunities for the development of new mapping approaches to detect rice using the Commission Internationale de l'Eclairage (CIE) colour space, in which colours perceived by human eyes have specific numerical positions on the CIE chromaticity diagram (C.I.E, 1932). However, to the best of our knowledge, a methodology for mapping paddy rice according to its unique spectra (meaning unique colours observed in remotely sensed imagery) leveraging the CIE colour space has not yet been reported.

To fill this knowledge gap, for the first time, we propose an entirely new approach named RiceTColour for mapping paddy rice based on its unique spectra during transplanting using the CIE colour space. Our RiceTColour represents a new approach to rice mapping, addressing all of the above three challenges directly. Specifically, the advantages of our proposed RiceTColour method are (1) it has strong transferability capacity; (2) it is a parameter-less and threshold-less method and (3) it utilises just a single image or composite imagery collected during transplanting. The proposed RiceTColour method was validated on five rice-planting areas, encompassing diverse climates, irrigation scenarios and cropping systems.

2. Study area and data

2.1 Study area

A total of five typical rice-planting areas (Fig. 1) under distinct environmental conditions were selected carefully to test comprehensively and thoroughly the effectiveness and generalisability of the developed RiceTColour rice mapping approach. These regions differ greatly in terms of their climates (tropical, cold, arid, temperate and subtropical), rice crop intensities (single-cropping and double-cropping), irrigation scenarios (surface water-fed and groundwater-fed) and crop rotations (rice-rice, rice-other and rice-fallow) (Table 1).

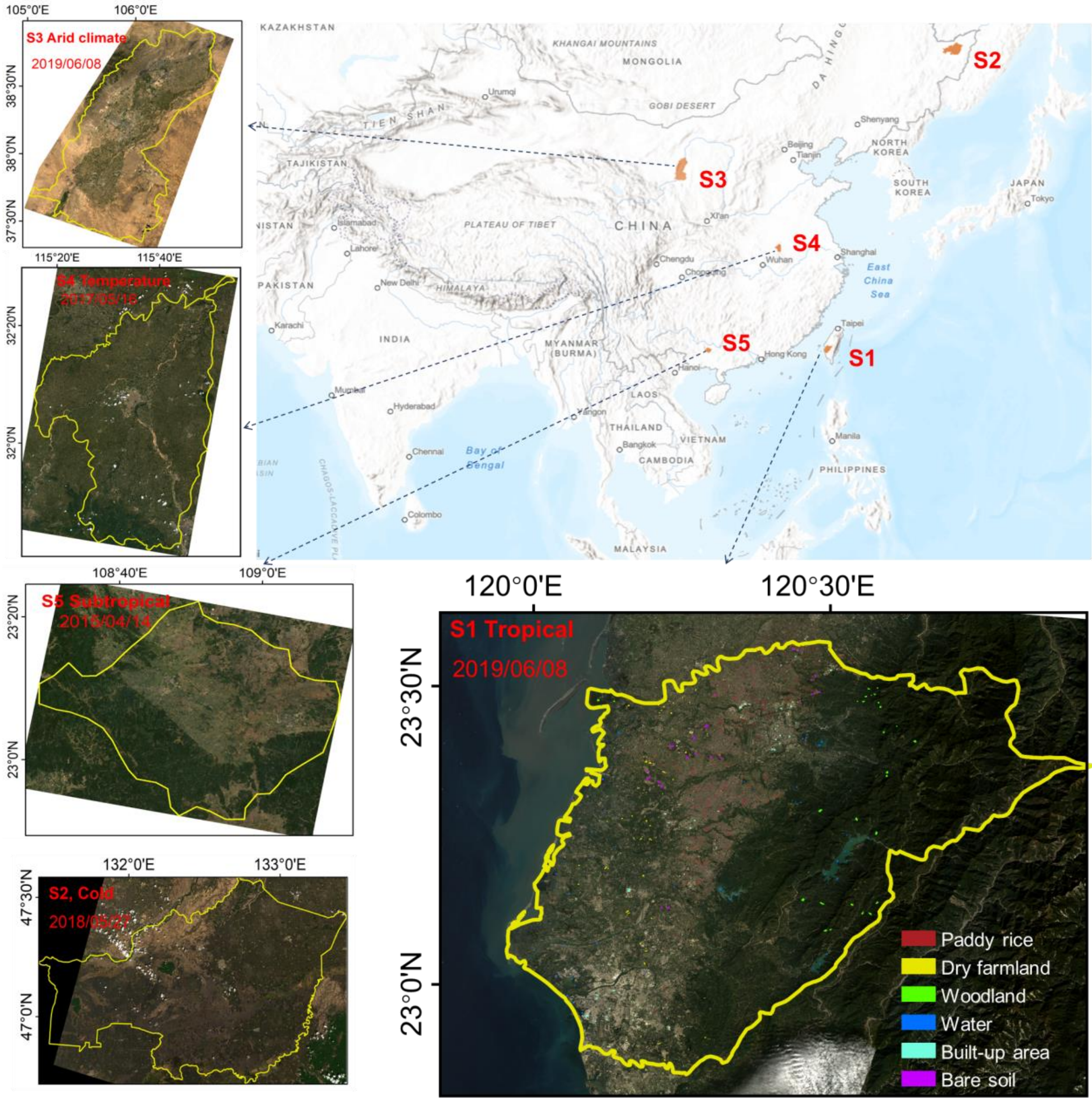

Figure 1. Geographical locations of the five study areas: S1, Chiayi and Tainan counties, Taiwan Island; S2, Fujin county, Heilongjiang Province; S3, Yinchuan and Shizuishan cities, Ningxia Autonomous Region; S4, Gushi county, Henan Province; S5, Binyang county, Guangxi Autonomous Region. Details of each study area are displayed by true-colour Landsat 8 imagery. Note that S1 was enlarged to demonstrate the training polygons for rice and other land covers.

The first study area (S1), comprising two counties (Chiayi and Tainan), is located in the southwest of Taiwan Island, with a total area of 4,155 km^2. The western region of S1 is the Chianan Plain, while the eastern region is dominated by mountain ranges. S1 is characterised by a tropical climate, with an annual mean temperature over 24°C and annual precipitation of approximately 2,000 mm (Son et al., 2021). There are two distinct seasons, a summer wet season lasting from May to October and a winter dry season spanning the remaining months (Huang et al., 2021). Although the eastern region is dominated primarily by mountain ranges, the majority of the western Chianan Plain is cultivated as farmland. Rice is the major crop in this region, encompassing approximately a quarter of the total farmland area. It generally transplanted from January to March and harvested in June and July during the wet season, and transplanted in July and August and harvested in November and December during the dry season. The primary source of irrigation water in this area comes from reservoirs, supplemented by rivers and underground water. In addition to rice, vegetables, orchards and fruit trees are also widely distributed across this region. Being managed by smallholder farmers, the farmland fields here are relatively small, with an average size of rice field of ~0.2 ha, scattered across the Chianan Plain.

Table 1. Summarised descriptions of the five study areas.

Study areas	**Location**	**Climate**	**Major crop categories**	**Area (%) of crops to study area**	**Irrigation sources**	**Rotation systems**	**Cropping intensities**
S1	Chianan Plain	Tropical	Rice, orchards and fruit trees (OFT), and vegetables (VT)	Rice: 11.07% OFT: 13.08% VT: 5.37%	Reservoirs and rivers	Rice-Rice Rice-Other	Double
S2	Sanjiang Plain	Cold	Rice and corn	Rice: 39.70% Corn: 16.09%	Rivers and underground water	Rice-Fallow	Single

S3	Yinchuan Plain	Arid	Rice, corn and spring wheat (SW) and fodder crops (FC)	Rice: 5.56% Corn: 4.82% SW: 2.15% FC: 1.26%	Rivers	Rice-Fallow	Single
S4	Middle-lower Yangtze Plain	Temperate	Rice and spring wheat	Rice: 39.28% SW: 12.56%	Reservoirs	Rice-Fallow	Single
S5	Nanning Basin	Subtropical	Rice, sugarcane (SC), corn and sweet potato (SP)	Rice: 12.23% SC: 8.16% Corn: 3.49% SP: 1.33%	Reservoirs	Rice-Rice Rice-Other	Double

The second to fifth (S2 to S5) study areas are located in the mainland of China, specifically in Sanjiang Plain, Northeast (NE) China (S2), Yinchuan Plain, Northwest (NW) China (S3), Middle-lower Yangtze Plain, Central and East (CE) China (S4), and Nanning Basin, South China (S5). The total areas of S2 to S5 are 8,227 km^2, 14,335 km^2, 2,946 km^2 and 2,314 km^2, respectively. They represent typical rice-planting areas distributed across China. For example, S2 (Fujin county) and S4 (Gushi county) are the largest rice-planting counties in Heilongjiang and Henan provinces, respectively, while S5 (Binyang county) is the second-largest rice-planting county in the Guangxi Autonomous Region. Amongst the four study areas, S2 to S4 are dominated by single rice cropping with similar rice planting calendars, involving seeding and transplanting in spring and harvesting in autumn. However, as the three regions are situated at different latitudes across the mainland of China from north to south, they experience disparate climates, characterised as cold (S2), arid (S3), and temperate (S4), respectively (Beck et al., 2018). In contrast, with a humid subtropical climate, the rice in S5 is typically cultivated twice a year, with the first-season rice being planted during March to April, followed by the second-season rice in June to July. Temperature and precipitation vary greatly amongst the four areas. With hot and rainy summers and cold and dry winters, S2 has an average annual temperature of 2.6℃ and annual precipitation of 536 mm, with the length of frost-free days ranging from 130 to 140 days. Located in an arid region, S3 experiences a relatively small average annual precipitation of only 188 mm, which is just one-tenth of its annual evaporation amount (1825 mm) (Zhang et al., 2022). In contrast, located in the Pishihang Irrigation District, the annual precipitation in humid S4 is markedly greater, measuring about 1287 mm, accompanied by an average temperature of approximately 15 °C. Similarly, the temperature and precipitation in S5 are sufficient for rice production, as substantiated by an average annual temperature of 20.8 °C and an annual rainfall of 1589.2 mm. The four sites also have varying terrain conditions. While the terrain is almost flat across S2 to S4, they differ significantly in altitude, with an average altitude between 1100-1200 m for S3, and 60-80 m for S2 and S4. In contrast, the terrain in S5 is a mixture of plains, hills and mountains, with an average altitude ranging between 100-120 m. Different natural conditions over S2-S5 have resulted in different crop planting structures and irrigation schemes. Specifically, the agricultural landscapes of S2 and S4 are quite simple, dominated by paddy rice. In contrast, the remaining two sites exhibit a relatively complex landscape with four major crops according to our field investigations: paddy rice, corn, spring wheat and fodder crops for S3, and paddy rice, sugarcane, corn and sweet potato for S5. The proportion of paddy fields to the total cropland area for S2 to S5 is 89.54%, 20.06%, 76.65% and 20.91%, respectively. Regarding the irrigation schemes, the primary sources of irrigation water in S2 come from both the Songhua River and underground water extracted by pumps. Based on irrigation networks, rice fields in S3 are predominantly irrigated from the Yellow River, while those in both S4 and S5 primarily rely on reservoir water for irrigation (Table 1).

2.2 Data

2.2.1 Ground reference data

To observe the patterns of crop fields, a typical rice planting area was selected for each study area and the corresponding very fine resolution (VFR) remote sensing image was acquired from Google Earth Pro (Fig. 2). As can be seen from the figure, the rice fields in tropical S1, with typically rectangular shapes, are relatively small, fragmented and scattered, often intermixed with diverse dry farmland crops and land cover types. Similarly, the rice fields in temperate S4 and subtropical S5 are also small and fragmented, but they lack regular shapes. In contrast, the agricultural landscapes in the cold S2 and dry S3 are relatively homogeneous, characterised by large and regular-shaped rice fields due to a very high level of agricultural mechanisation (Chen et al., 2022). Considering the complicated and heterogeneous agricultural landscape in S1, we conducted the analysis and demonstration of spectra for paddy rice and other land cover types in S1. The remaining study areas (S2 to S5) are employed to validate the transferability of our developed rice mapping approach. We hypothesize that if the proposed method can identify accurately paddy rice over complex regions like S1, it should also work effectively in other rice planting regions.

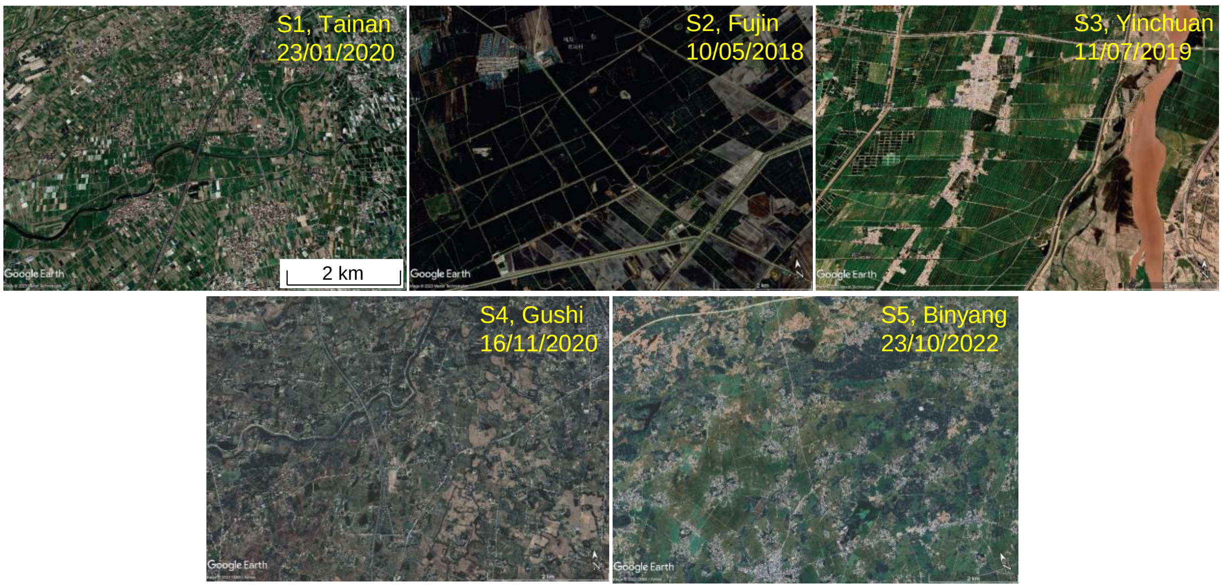

Figure 2. Very fine resolution remotely sensed imagery over typical rice-planting area in each study area. The location and acquisition date are labelled in each image. Note that all the images are at the same spatial scale.

The ground reference data (training and validating sample plots) for the study areas were collected through reference rice maps, field surveys and VFR images (such as Google Earth (GE) VFR data). Note that the training samples were collected only from S1 to establish the rice mapping models, whereas the validating samples were acquired in each of the five study areas to assess the effectiveness of the models. A stratified random sampling scheme was used to acquire the training samples. Specifically, a total of 378 training polygons were identified, including 188 field patches for paddy rice and 190 for other land covers. The paddy rice polygons were selected randomly according to a set of Taiwan rice distribution (TRD) maps generated by the Council of Agriculture Executive Yuan of Taiwan, while those for other land covers were obtained in reference to the VFR images. Note that the TRD maps were produced through digitizing aerial remote sensing photos and were comprehensively validated using field survey data, thus, possessing very high accuracy (Son et al., 2021). The training polygons were subsequently overlaid with the Landsat 8 data, and the pixels falling within the training polygons were utilised as training samples, resulting in 3,503 rice sample plots and 7,842 non-rice sample plots (including 1,216 dry farmland, 2,303 woodland, 1,509 water, 1,203 built-up area and 1,611 bare soil). These training sample plots were employed to visualize the distribution patterns of paddy rice and other land covers in the CIE colour space, based on which the separation boundaries between rice and other land covers were determined, as elaborated in detail in the following methodology section.

To validate extensively the effectiveness of the proposed method, validation samples were collected in each of the five study areas using a stratified random sampling scheme. Following the recommendations by Stehman and Foody (2019), the sample size (n) was determined using the following formula:

$$n = \frac{z^2 p(1-p)}{d^2} \tag{1}$$

where p denotes the expected overall accuracy (expressed as a proportion), d represents the desired half-width of the confidence interval, and z is a corresponding percentile from the standard normal distribution (e.g., z=1.96 for a 95% confidence interval). Rice mapping is a binary classification, and we anticipate that classified maps should have very high confidence. In our experiments, the d was set as 0.02 (i.e., a 98% confidence interval), with the corresponding z value of 2.33. Besides, the p was set as 0.5 to acquire as many validation samples as possible. As a result, a total of 3393 validation samples (determined using Eq. (1)) were collected for each study area. For S1, the rice and non-rice validation samples were acquired according to the TRD map and Google Earth VFR images, respectively. For the remaining study areas (S2 to S5), validation samples were obtained through both field surveys and interpretation of VFR images. The number of samples for rice and non-rice classes in each study area was strictly proportional to the total area of each class.

2.2.2 Rice calendar data

The proposed RiceTColour method is based on the unique spectra of paddy rice fields exhibited in remote sensing images during the transplanting period. The method, thus, depends on knowledge of the rice calendar. In this research, the phenological stages of paddy rice in each study area are classified into three categories: transplanting, growing and harvesting, as summarised and demonstrated in Fig. 3. As can be seen from the figure, that the timing of paddy rice transplanting varies greatly across the five study sites, spanning from January in S1 to August in both S1 and S5. Specifically, the duration of transplanting is considerably longer in tropical S1 (first rice) and temperate S4, typically around 2.5 months, while relatively shorter in cold S2, dry S3 and subtropical S5 (both first and second rice), lasting about 1.5 months.

The rice growing period lasts for approximately four months in both S2 and S3 because of their relatively low annual average temperature, whereas paddy rice in the remaining sites (S1, S4 and S5) matures in only around three months thanks to the warm climate.

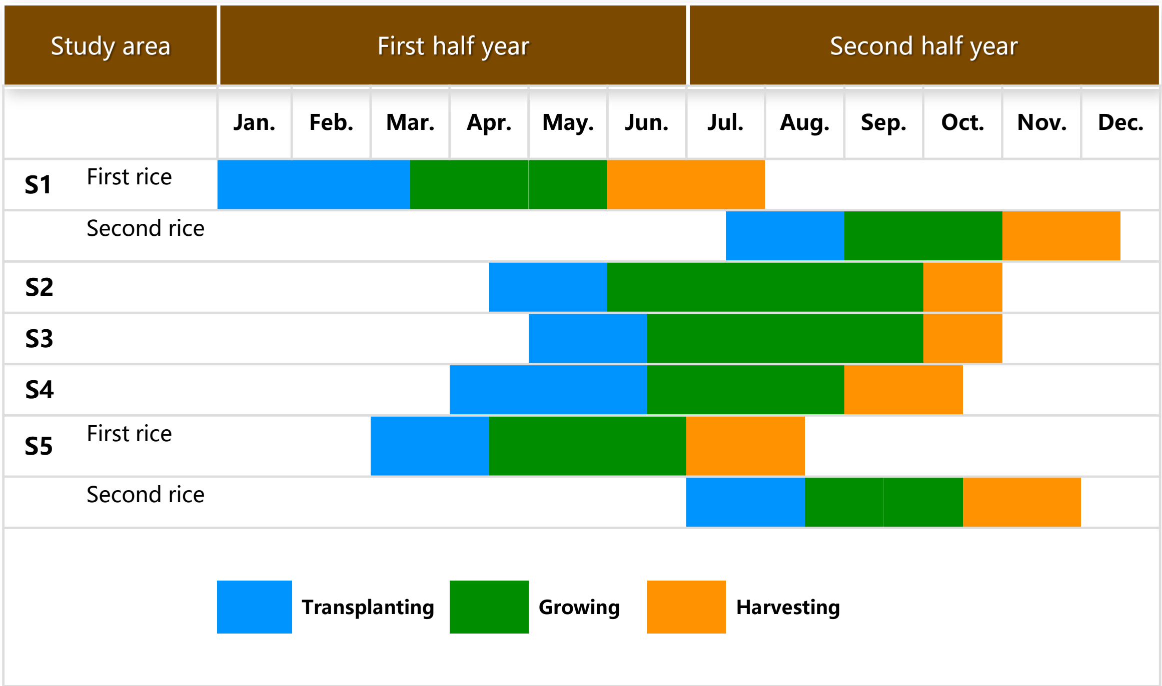

Figure 3. Rice calendars for the five study areas.

2.2.3 Satellite sensor data

In this research, the USGS Landsat 8 Collection 1 (C1) Surface Reflectance Tier 1 products (T1_SR) available in the Google Earth Engine (GEE) cloud computing platform were obtained and employed for paddy rice mapping. The Landsat Tier 1 products are of the highest data quality amongst the Landsat products since they are generated using only those images that meet standard geometric and radiometric quality criteria (Wulder et al., 2019). The products are made at a 30 m spatial resolution using specialized software named the Land Surface Reflectance Code (LaSRC) developed by NASA (Sayler, 2020). With calibration parameters from the metadata, LaSRC generates Landsat Top of Atmosphere (TOA) reflectance data, to which atmospheric correction routines are further applied using auxiliary input data (e.g., water vapor data, terrain data, etc.). The SR products include a Pixel Quality

Assessment (pixel_qa) band in which cloud, cloud shadow and snow/ice features are flagged using the CFMASK (C code Function of Mask) algorithm (Sayler, 2020).

To collect Landsat 8 data, we checked the availability of cloud-free T1_SR products for each study area collected during the transplanting period on GEE (Table 2). Cloud-free single images were available in both S3 and S5 where the weather often remains clear in spring. However, acquiring cloud-free images over the remaining three areas was extremely difficult, especially the rainy and cloudy S1 and S4 where sunny days are rare. We, therefore, employed single images in S3 and S5 and composite images in S1, S2 and S4 for rice mapping. To test the robustness of the rice mapping methods, the selected images for each study site were collected in different years (from 2015 to 2020). Details of the Landsat 8 image acquisitions used in this research are given in Table 2.

Table 2. Details of Landsat 8 and Sentinel-1 image acquisitions for rice mapping.

Study site	Year	Landsat 8		Sentinel-1			
		Date of acquisitions	Type of imagery	Acquisition period	Number of observatoins	Orbit	Incidence angle (°)
S1	2020	21/01, 06/02, 22/02	Composite	02/01-27/12	30	Descending	37.30-42.34
S2	2018	27/05, 03/06	Composite	03/01-29/12	31	Descending	32.54-41.62
S3	2019	08/06	Single-date	11/01-25/12	30	Ascending	36.79-44.89
S4	2017	30/04, 16/05	Composite	01/01-27/12	26	Ascending	38.31-41.93
S5	2015	14/04	Single-date	-	-		

In addition to Landsat 8, Sentinel-1 SAR data were collected over the study areas for comparison. Sentinel-1, equipped with a single C-band SAR instrument, was launched by the European Space Agency (ESA) in 2014 (Zhan et al., 2021). In this study, year-round Sentinel-1 Ground Range Detected (GRD) SAR data covering S1 to S4 were accessed from Google Earth Engine (GEE), with approximately 30 valid observations for each area (Table 2). The GRD data were calibrated and ortho-corrected dual polarization (VV/VH) products, with a spatial resolution of 10 m (Xu et al., 2023). The SRTM DEM or the ASTER DEM for high latitudes (> 60° or < -60°) were employed during the ortho-correction process to convert data to backscatter coefficient. Due to the unavailability of SAR data for the period from January to May in S5, this region was excluded from SAR-based rice mapping.

3. Methodology

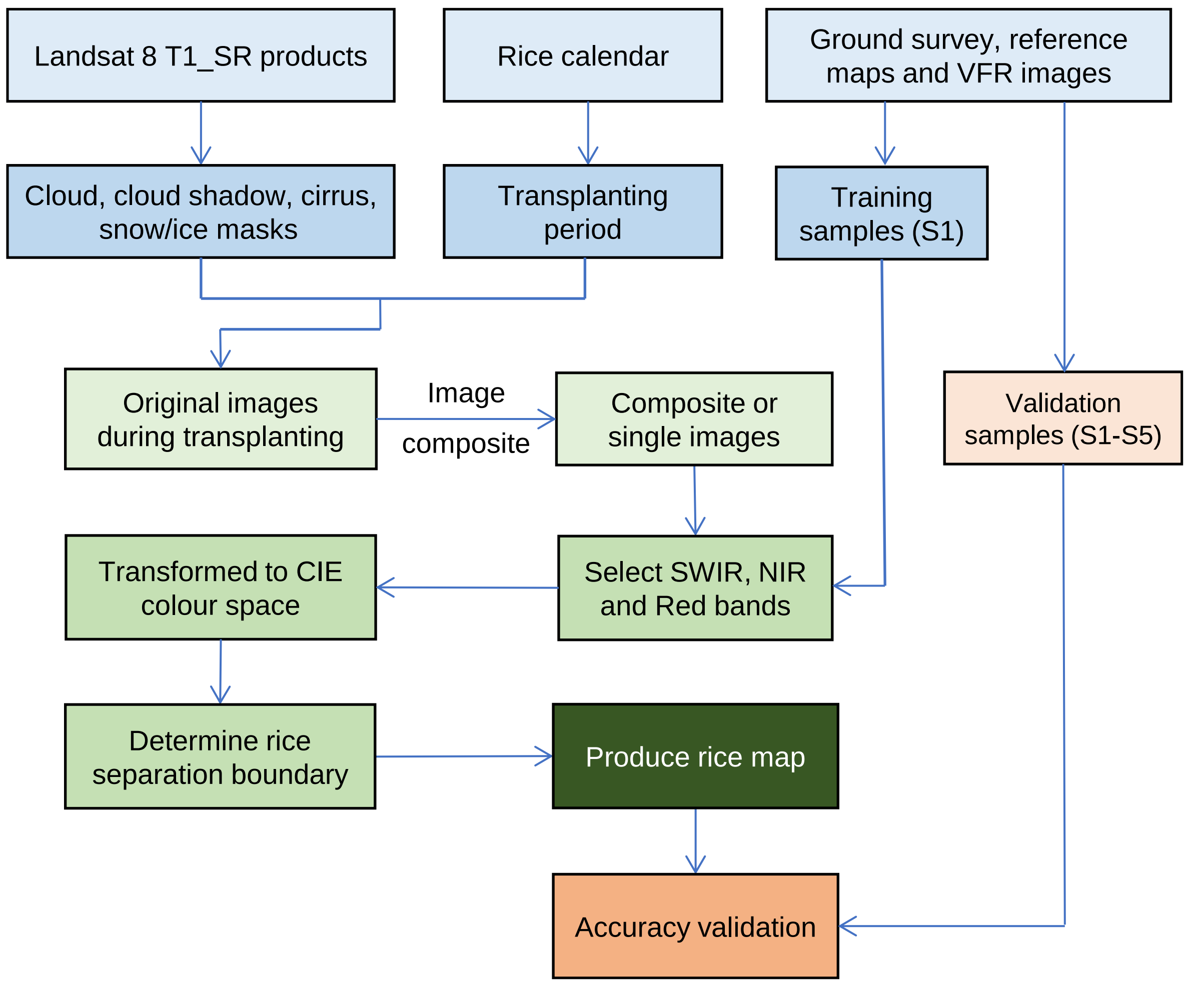

Figure 4. Workflow of the proposed RiceTColour method for rice mapping.

In this research, we proposed an entirely new method named RiceTColour to detect paddy fields based on their unique spectra during the transplanting period using the CIE colour space. The workflow of the RiceTColour is demonstrated in Fig. 4 and elaborated in detail as follows.

3.1 Unique spectra and colours of rice fields during the transplanting period

Different from upland crops that are seeded directly in soil, rice is the only crop that is transplanted (or seeded) and grown in flooded soil, a mixture of water and soil (Le Toan et al., 1997; Xiao et al., 2002; Dong et al., 2015). A few weeks after transplanting the rice plants will grow large enough to fully cover the rice fields, and no discernible signal differences can be detected between rice and upland crops during canopy closure in remote sensing imagery (Dong et al., 2016). Therefore, the transplanting stage, characterised by an open rice canopy and a unique soil-water-rice mixture environment, is crucial for differentiating rice from other crops (Zhan et al., 2021).

Spectral ranges of paddy rice and other land covers in the visible, near infrared (NIR) and shortwave infrared (SWIR) bands in S1 are demonstrated in Fig. 5. As can be seen from the figure, paddy rice presents unique spectra in the SWIR (an indicator of moisture) and NIR (an indicator of greenness) bands. Due to the moist backgrounds, the reflectance values of both paddy rice and water are relatively low (mainly lower than 0.05) in the SWIR bands, and they are generally lower than those of other land covers, especially in the SWIR1 band (Fig. 5 (e)). Although most of the incident infrared light is transmitted and reflected through the uppermost leaves of vegetation, the NIR values of paddy rice are also relatively low (mainly from 0.10 to 0.15) compared to those of other land covers due to its small amount of vegetation (rice seedlings). However, they are higher than those of water with smooth surfaces (Fig. 5 (d)).

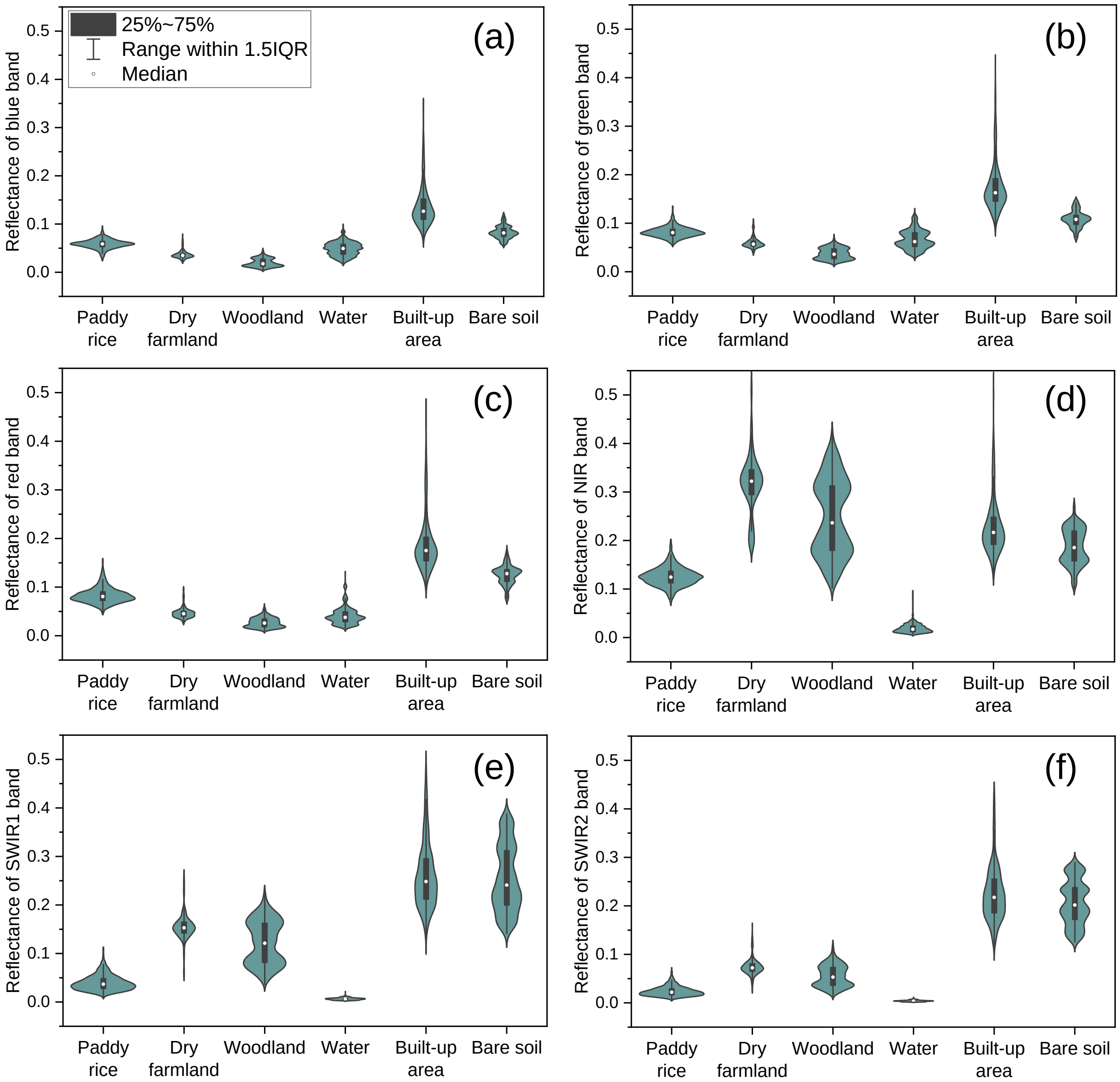

362

363 Figure 5. Box plot and violin plot depicting the reflectance of paddy rice and the other land covers in

364 visible, NIR and SWIR bands. Box plot consists of black rectangle and vertical lines and white median,

365 which are surrounded by the dark cyan violin plot.

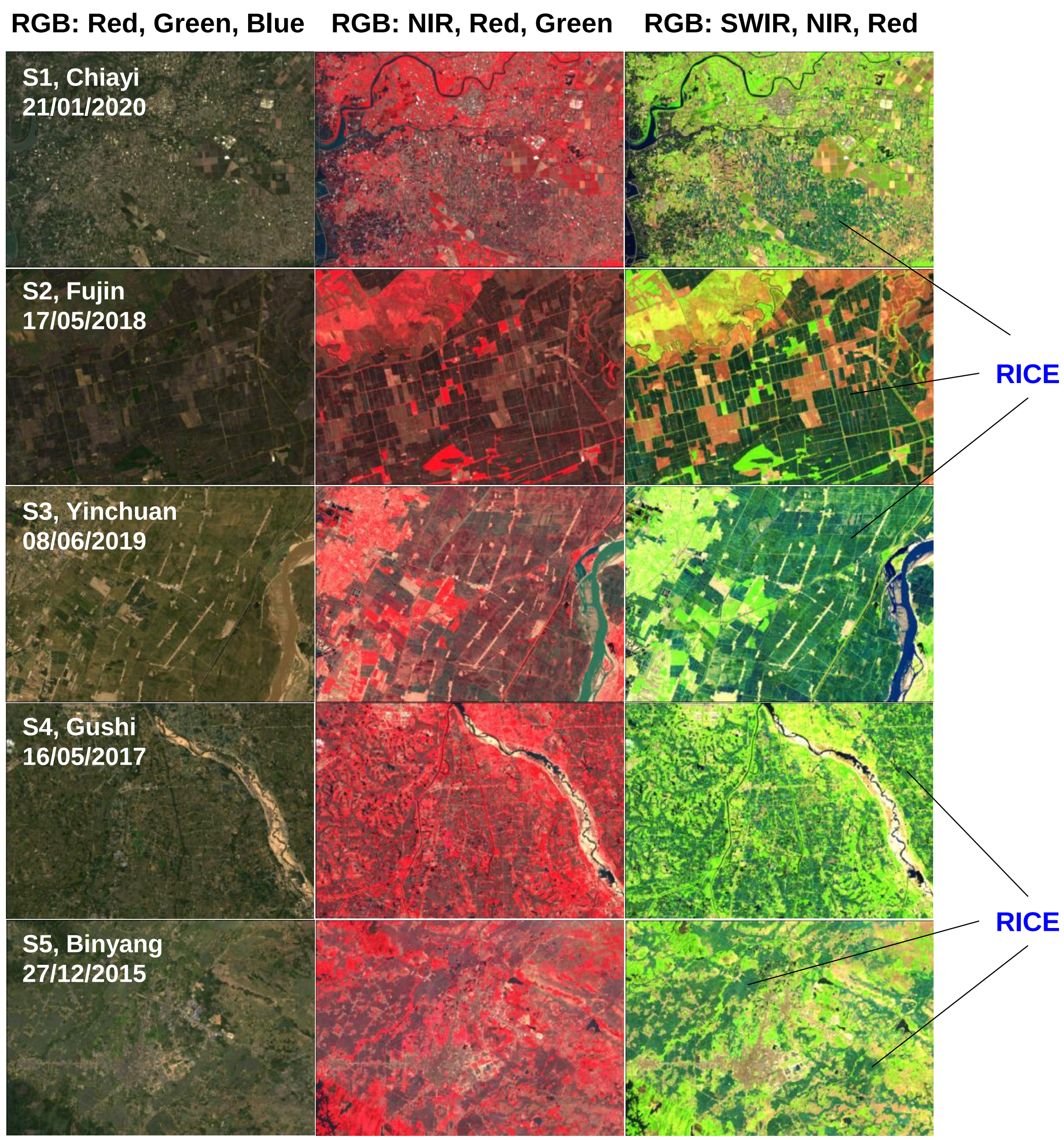

Figure 6. Typical images of the five study sites composed of different spectral bands. The images in the left, middle and right columns are comprised of Red, Green and Blue (true-colour image), NIR, Red and Green (false-colour image), and SWIR, NIR and Red (false-colour image), respectively.

The rich spectral bands contained in Landsat imagery enable the generation of different types of composite image for visual interpretation. These include a true-colour composite image displaying natural colours by utilising the Red, Green and Blue bands as the red, green and blue channels, respectively, and false-colour composite images showing non-natural colours by employing band combinations different from those used in the true-colour image (Patra et al., 2006). In consideration of the unique spectra of paddy rice in SWIR and NIR bands during the transplanting period as mentioned above, the SWIR1 (hereafter SWIR), NIR and Red bands were selected and utilised as the red, green and blue channels, respectively, to demonstrate the image. The Red band was selected because it has been widely demonstrated to be sensitive to vegetation biomass and leaf area index (LAI) (Heiskanen, 2006). As can be seen from Fig. 6, we discovered and confirmed that transplanted paddy rice fields exhibit unique dark green colours in false-colour composite imagery, composed of the SWIR (R), NIR (G) and Red (B) bands, as expected. Based on these specific colours, it is straightforward and easy to discern rice fields from other land covers in the imagery (right column of Fig. 6), which provides the basis for developing novel rice mapping methods using the CIE colour space. For comparison, we also demonstrated the true-colour imagery and the commonly-used false-colour imagery (RGB: NIR, Red, Green). However, we observed that visually discerning transplanted rice fields in both images is very challenging (left and middle columns of Fig. 6) as they display similar colours to other land covers.

3.2 Rice mapping within the CIE colour space

Based on the unique colours displayed by transplanted rice fields, this research proposes an entirely new method for rice mapping within the colour space created by the International Commission on Illumination (abbreviated as CIE according to its French name, Commission Internationale de l'Eclairage) in the year of 1931 (C.I.E, 1932). The main idea of the method is to establish classification criteria to differentiate paddy rice from other land covers through analysing the spatial distribution patterns of training samples of paddy rice as well as other land covers within the CIE colour space. The greatest advantage of the CIE colour space is that it enables the transformation of any colour composed of the traditional three tristimulus values (RGB: red, green and blue) into a quantified two-dimensional (2D) colour space (C.I.E, 1932; Shen et al., 2019). In other words, any colour observed in remote sensing imagery by the human eye has a specific numerical position within the CIE colour space, which lays the foundation for quantitatively characterising colour (class) similarities (Fig. 7 (a)).

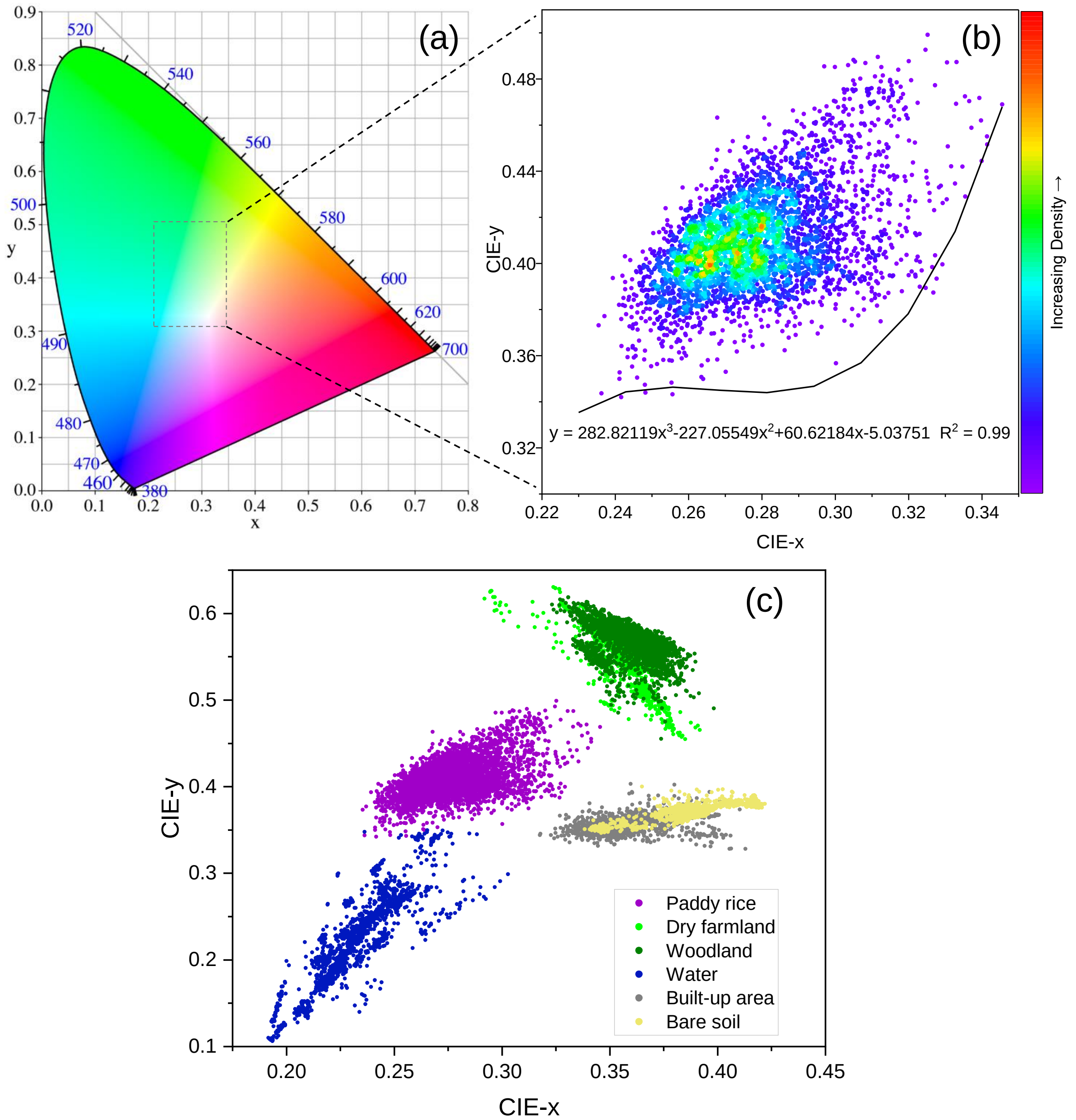

Figure 7. (a) An illustration of the CIE chromaticity diagram (i.e., colour space). (b) Point density map of the training samples for paddy rice in S1 within the CIE colour space. (c) Scatterplots of the training samples for paddy rice and the other five land covers (dry farmland, woodland, water, built-up area and bare soil) in S1 within the CIE colour space.

The conversion of the three tristimulus values within the RGB colour space to the 2D CIE chromaticity coordinates (x, y) can be achieved using the following equations:

$$x = X/(X + Y + Z) \tag{2}$$

$$y = Y/(X + Y + Z)$$

$$X = 2.7689R + 1.7517G + 1.1302B$$

$$Y = 1.0000R + 4.5907G + 0.0601B$$

$$Z = 0.0000R + 0.0565G + 5.5943B$$

where R, G and B represent the red, green and blue bands, respectively; x and y represent the X and Y coordinates of the CIE colour space.

As mentioned above, rice fields are distinguishable in the false-colour image composed of the SWIR, NIR and Red bands of Landsat 8 imagery, rather than in the true colour image (Fig. 6). As such, in this research the SWIR (band 6, 1570–1650 nm), NIR (band 5, 850–880 nm) and Red (band 4, 640–670 nm) bands were employed, respectively, as the R, G and B bands to transform the observed colours into the CIE colour space using Eq. (2). Paddy rice, with its unique dark green colours, is expected to occupy specific areas within the CIE colour space so that it can be differentiated from other land covers. Based on the collected training samples in S1 (section 2.2.1), we first extracted the reflectance values of the three used bands (i.e., SWIR, NIR and Red) for each sample point. Subsequently, we transformed the extracted values of each point into the 2D CIE colour space using Eq. (2), and generated scatterplots for paddy rice and the other five land covers (dry farmland, woodland, water, built-up area and bare soil), as demonstrated in Fig. 7 (c). It is encouraging to observe from the figure that paddy rice is visually distinguishable and can be separated fully from the other land covers within the CIE space (Fig. 7 (c)), except for a very tiny overlap between paddy rice and water. As expected, nearly all of the sample points for paddy rice fall within the greenish gamut of the CIE chromaticity diagram (Fig. 7 (a)), which is consistent with the dark green colours of transplanted paddy rice exhibited in the SWIR-NIR-Red false-colour composite imagery (the images in the right column of Fig. 6).

To separate paddy rice from the other land covers within the CIE space, we established the lower boundary for the scattered points of paddy rice. This boundary corresponds to the lightest green colour of the selected paddy rice samples, and points above it correspond to paddy rice pixels displaying darker and greener colours. A polynomial regression boundary was generated and fitted to the sample points of paddy rice. First, we identified all of the convex hull vertices (points) of the paddy rice samples. Second, the vertices with the minimum and maximum x-coordinate values were selected to form a line, and the vertices above the line were deleted. Third, a third-order polynomial regression was produced by fitting the remaining vertices (Fig. 7 (b)). The established polynomial regression boundaries are as follows:

$$y_{\mathrm{lower}} = 282.82119x^3 - 227.05549x^2 + 60.62184x - 5.03751 \quad (3)$$

In the equation, the coefficients of the cubic term, quadratic term and linear term determine the curve's opening direction, shape and position, respectively. Herein, 282.82119 and 60.62184 are both positive, resulting in the curve opening upwards, while -227.05549 is negative, leading to a valley shape for the curve.

As can be seen from Fig. 7 (c), the sample pixels of paddy rice are distributed within specific ranges within the CIE space: 0.235 to 0.346 along the x coordinate axis, and below 0.5 along the y coordinate axis. We, therefore, classify each candidate pixel (x, y) of remotely sensed imagery as paddy rice if it satisfies the following criteria within the CIE space:

$$y_{\mathrm{lower}} < y < 0.5 \quad \text{and} \quad 0.235 < x < 0.346 \quad (4)$$

3.3 Practical workflow for rice mapping with the RiceTColour method

The practical workflow of the proposed method consists of the following three steps (Fig. 4):

First, remove contaminated pixels (noise) from the remotely sensed imagery since they can impact the rice mapping results. In this research, pixels of Landsat 8 imagery contaminated by cloud, cloud shadow and snow/ice were first identified and eliminated using the ‘pixel_qa’ band. Cirrus clouds may also affect the reflectance of Landsat 8 data (Qiu et al., 2020) and, thus, pixels contaminated by cirrus clouds were also removed from further analysis.

Subsequently, any saturated pixels were removed using the ‘radsat_qa’ band, although saturation is uncommon in Landsat 8 imagery. Besides, a few pixels were occasionally found to exhibit abnormally negative reflectance values in one or more spectral bands (bands 2 to 7). These were identified as contaminated pixels and removed from subsequent analysis. Additionally, in practice we observed that open water can be easily misclassified as transplanted rice fields due to their similar spectral characteristics. To mitigate such interference in rice mapping, we excluded open water from the remotely sensed imagery using a commonly-used threshold method: any pixel with an NDVI lower than 0 was identified as water and removed from subsequent analysis (Jarchow et al., 2017).

Second, image compositing was undertaken using a pixel-based minimum SWIR method. In tropical and temperate regions, it is challenging to collect cloud-free remotely sensed imagery during the rice transplanting period. Importantly, due to the differences in natural conditions and farmer’s management practices, the timing of transplanting always varies greatly across rice fields. It is often difficult to capture transplanting signals for all rice fields using a single-date image. Consequently, image compositing is generally necessary to produce cloud-free imagery for rice mapping. Since the SWIR is highly sensitive to water content (Tian and Philpot, 2015), it is considered as the primary indicator of transplanted paddy rice fields. Herein, a pixel-based minimum SWIR (i.e., maximum water content) composite method (PMS-CM) was applied to the collected images to generate composite imagery. Specifically, for each pixel of an image, the one with the minimum SWIR value across the collected image time-series was selected to constitute the composite image. By doing this, the most significant signal (i.e., the maximum water content) of each pixel in rice fields can be captured. Nevertheless, in regions where cloud-free single images are available, there is no need to perform the image composite procedure.

Third, paddy rice mapping within the CIE colour space. Select the three bands (i.e., SWIR, NIR and Red) from the processed composite imagery (or single imagery), and transform reflectance values into the 2D CIE-colour space using Eq. (2) for each pixel of imagery. Based on the established paddy rice classification criteria (Eq. (4)), a rice map is produced for each study site.

3.4 Benchmarks and accuracy assessment

In this research, the effectiveness of the proposed rice mapping approach (RiceTColour) was evaluated against four other benchmark methods: a SAR-based method, an index-based method and two supervised classifier-based methods. For the SAR-based method, the recently proposed Automated Rice Mapping using Synthetic Aperture Radar Flooding Signals (ARM-SARFS) was adopted due to its superior performance over other SAR-based methods (Zhan et al., 2021). ARM-SARFS includes four pre-defined thresholds, namely T1, T2, T3 and T4. The first two are designed to mask out non-cropland land covers, while the last two are used to differentiate paddy rice from other crops. In our experiments, the optimal values for T1 and T2 for each study area were tuned using a grid search from -30 to -10 with a step size of 1. The optimal combinations of T1 and T2 for S1 to S4 were found to be -20 and -23, -25 and -25, -25 and -25, and -20 and -20, respectively. T3 and T4 are fixed thresholds dependent on rice type (early rice, middle rice and late rice), and the recommended values by Zhan et al. (2021) were adopted directly for rice mapping. For the index-based method, we selected the normalized difference water index (NDWI), which is calculated as the normalized difference of the green band (i.e., band 3 of Landsat 8) and SWIR band (i.e., band 6 of Landsat 8) (Ji et al., 2009). This is because previous studies demonstrated its superior performance in detecting rice fields compared with other vegetation indices (Boschetti et al., 2014). The threshold of NDWI was tuned from -0.30 to -0.10 with a step of 0.002 through cross-validation, and the optimal threshold was found to be -0.228, which was equivalent to that determined by Boschetti et al. (2014). For the supervised classifier-based method, the random forest classifier (RFC) and the one-class support vector machine (OCSVM) were adopted as comparators. To ensure a fair comparison, the SWIR, NIR and Red bands of Landsat 8 imagery were employed as input for both classifiers, consistent with the input of the proposed RiceTColour method. The RFC is intrinsically a tree-based ensemble classifier (Breiman, 2001), thus, performing relatively robustly in various crop mapping applications (Belgiu and Drăguţ, 2016). To ensure model stability, the number of trees for the RFC in our experiments was optimised as 200. The OCSVM, a variant of standard SVM, is designed specifically for one-class classification tasks (Schölkopf et al., 2001). The superiority of OCSVM for rice detection was demonstrated extensively by previous studies (Clauss et al., 2016; Ni et al., 2021; Zhang et al., 2021). Following the recommendations by Clauss et al. (2016), an OCSVM with a Radial Basis Function (RBF) kernel was applied in our experiments. The two vital parameters of OCSVM, γ and ν, which control the width of the kernel and the proportion of outlier samples for the target class, respectively, need to be determined carefully. Following the recommendations by Ni et al. (2021), the optimal γ and ν were optimised as 10 and 0.01, respectively, from (0.01, 0.05, 0.1, 0.5, 1, 2.5, 5, 10, 25) and (0.01, 0.05, 0.1, 0.5, 1, 2.5, 5, 10, 25) using a grid-search approach.

To evaluate quantitatively the accuracy of the produced rice maps, four metrics were employed, including the overall accuracy (OA), producer's accuracy (PA), user's accuracy (UA) and F_1-score (Foody, 2021). The F_1-score is a harmonic mean of PA and UA. Compared with OA, it can better indicate the model capability of identifying imbalanced classes (Zhong et al., 2019). Additionally, two mutually exclusive metrics, quantity disagreement and allocation disagreement (Pontius and Millones, 2011), were also adopted to measure quantitatively the differences between classified maps and the reference. They have been proven to be more reasonable and useful than the commonly-used Kappa coefficient, which is advocated for removal from classification accuracy analysis (Stehman and Foody, 2019).

4. Results and analysis

4.1 Rice mapping results by RiceTColour

The pixel-based minimum SWIR composite method was applied in S1, S2 and S4 to produce composite images for rice mapping, whereas for S3 and S5 single-date images were used for rice classification (Table 2). The mapping results produced by the proposed RiceTColour method along with the corresponding satellite sensor images over all five study sites are shown in Fig. 8. It can be seen from the figure that the produced rice maps are highly consistent with the spatial patterns of paddy rice fields (identifiable by their dark green colours) as observed in the satellite sensor images across the five study areas. This demonstrates the effectiveness and remarkable generalisation capability of the proposed method for rice detection over rice-planting regions under various natural conditions and management practices. Specifically, as can be interpretated visually from the satellite maps, although paddy rice is one of the major crops in S1, S3 and S5, it occupies a relatively small proportion of the total area in these regions due to the limited availability of arable land. Rice fields are primarily distributed in the western plains and central hills and plains in S1 and S5, respectively, with scattered fields in other regions. For S3, the rice fields are concentrated mainly in the northern region between Yinchuan City and Shizuishan City, with fragmented occurrences on both sides of the Yellow River in the southern area. Surprisingly, the spatial distribution of both the clustered and scattered rice fields were captured accurately and precisely by the RiceTColour method (Fig. 8). In contrast, the majority of areas in both S2 and S4 are occupied by rice fields. Rice fields in S2 are generally regular and large, and distributed contiguously due to the high level of mechanisation in the Sanjiang Plain (Chen et al., 2022). In contrast, those in S4 are irregular and highly fragmented due to the widely distributed road networks, towns and villages, and small ponds. Fortunately, the proposed RiceTColour method detected completely and precisely the clustered and dispersed patterns of rice fields in S2 and S4, respectively.

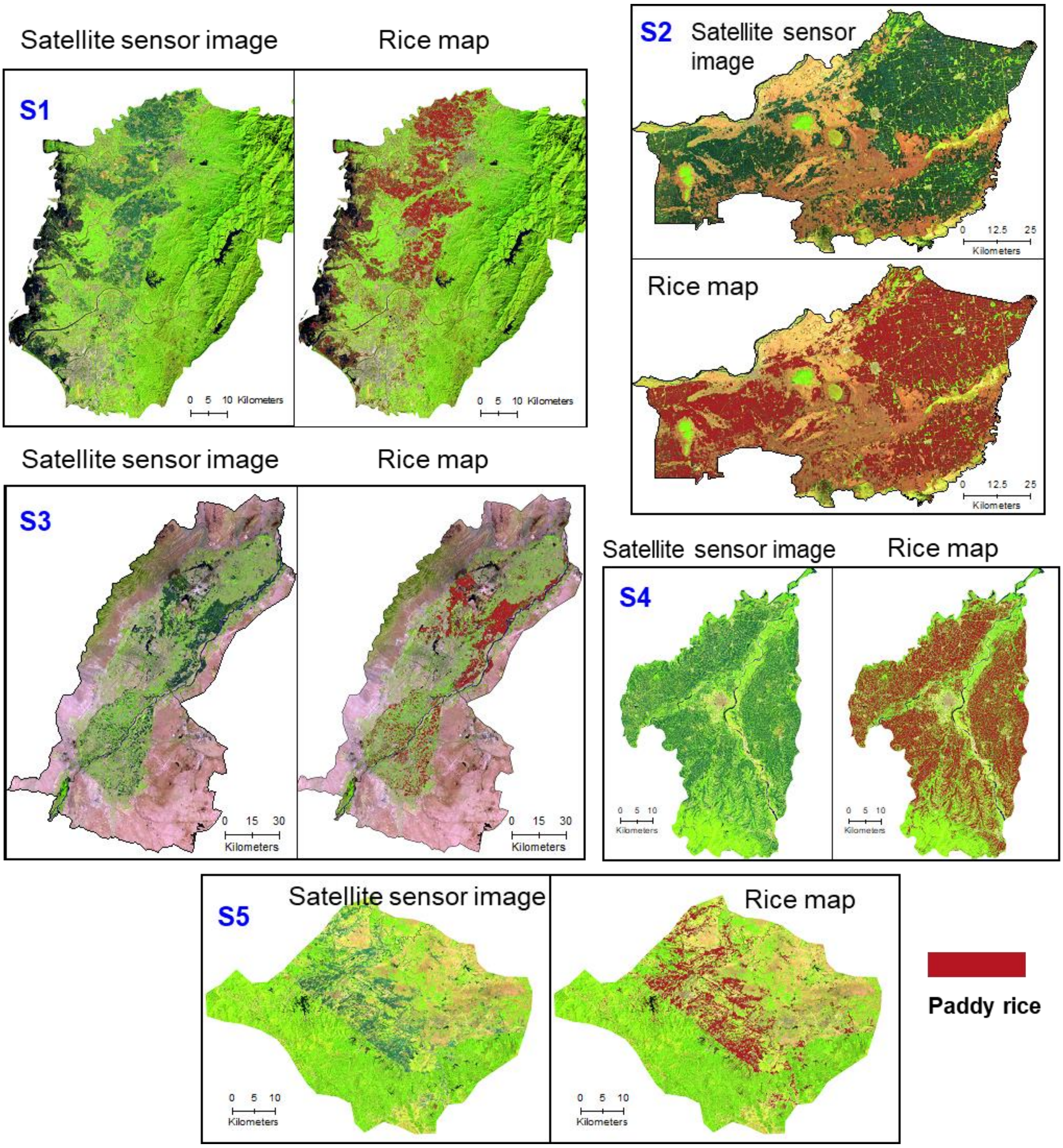

Figure 8. Rice mapping results by the proposed RiceTColour method and the corresponding satellite sensor images (RGB: SWIR, NIR, Red) over the five study sites.

Accuracy assessment of the rice maps was undertaken using the validation samples over the five study sites, and the confusion matrices along with the corresponding classification accuracies are listed in Table 3. As shown in the table, the RiceTColour method achieved very high mapping accuracies, with an OA above 95% for all study sites. Importantly, the RiceTColour method was highly stable across the five study sites, producing an OA of around 97% (ranging from 95.76% to 98.50%), demonstrating its remarkable generalisation capability for rice detection. Besides, it generated relatively balanced PA and UA for paddy rice, the target class of this research. The PA exceeded 92% at all study sties (except S3), indicating that nearly all (over 92%) of the rice fields in each study site were successfully detected by the proposed method. The UA of paddy rice was also greater than 90% for most of the sites (S2, S4 and S5), suggesting that just a small proportion of non-rice pixels were incorrectly labelled as paddy rice. The balanced rice mapping accuracies can be also observed from the F_1-score, which ranges between 0.87 and 0.97 across the five sites (Table 3).

Table 3. Confusion matrices of the classification maps produced by the RiceTColour method along with the corresponding classification accuracies in the five study sites.

Study site	Sample size (rice:non-rice)	Reference	Classification Rice	Classification Non-rice	PA	UA	Accuracy
S1	376:3017	Rice	348	61	92.55%	85.09%	OA = 97.38%
		Non-rice	28	2956			F_1-score = 0.89
S2	1347:2046	Rice	1300	47	96.51%	96.51%	OA = 97.23%
		Non-rice	47	1999			F_1-score = 0.97
S3	189:3204	Rice	169	31	89.42%	84.50%	OA = 98.50%
		Non-rice	20	3173			F_1-score = 0.87
S4	1333:2060	Rice	1285	71	96.40%	94.76%	OA = 95.76%

		Non-rice	48	1989			F_1-score = 0.96
S5	352:3041	Rice	334	37	94.89%	90.03%	OA = 98.38%
		Non-rice	18	3004			F_1-score = 0.92

4.2 Benchmark comparison for rice mapping

The rice mapping results of the proposed RiceTColour method were further benchmarked with four comparators (ARM-SARFS, NDWI, RFC and OCSVM) across the five study areas. Visual inspection as well as quantitative accuracy assessment was conducted to validate the rice mapping results of the five methods. To aid visual inspection, one-to-two typical rice-planting areas were selected at the five study sites for comparison. The original Landsat 8 satellite sensor images along with the mapping results of the various methods for these areas are shown in Fig. 9. As demonstrated by the figure, the proposed RiceTColour method consistently achieved the most accurate and desirable paddy rice maps across S1 to S5. For S1 (Fig. 9 (a) and (b)), it is evident that ARM-SARFS failed to identify a substantial number of rice fields, while both NDWI and RFC misclassified a significant portion of built-up areas and fish ponds as paddy rice. Besides, NDWI, RFC and OCSVM frequently misidentified roads within and outside farm fields as paddy rice. In contrast, the RiceTColour method differentiated accurately paddy rice from built-up areas, fish ponds and road networks (clearly observable on the map) (Fig. 9 (a) and (b)). For the generalised study areas (S2 to S5), SAR-based ARM-SARFS produced inaccurate rice classification maps, missing a significant proportion of rice fields, particularly in S3. Although the remaining three comparators (NDWI, RFC and OCSVM) performed more accurately than ARM-SARFS, NDWI tended to overestimate paddy rice, while both RFC and OCSVM were prone to underestimating paddy rice (Fig. 9 (c), (d), (f), and (g)). For example, the majority of the river in S2, as well as parts of the built-up areas in S2 and S4, were misidentified as paddy rice by NDWI. NDWI overestimated paddy rice increasingly seriously in S3, where large areas of dry farmland, built-up area and bare soil were wrongly labelled as paddy rice (Fig. 9 (d) and (e)). On the contrary, OCSVM omitted a relatively large portion of paddy rice in S2, S3 and S5, as well as the edges of most rice fields in S4. Although RFC was better than OCSVM in mitigating underestimation, it still failed to detect a number of small-area rice fields across S2 to S4. The proposed RiceTColour method, surprisingly, rectified almost all of the abovementioned misclassifications and detected rice precisely and completely, as demonstrated by Fig. 9 (c) to (g).

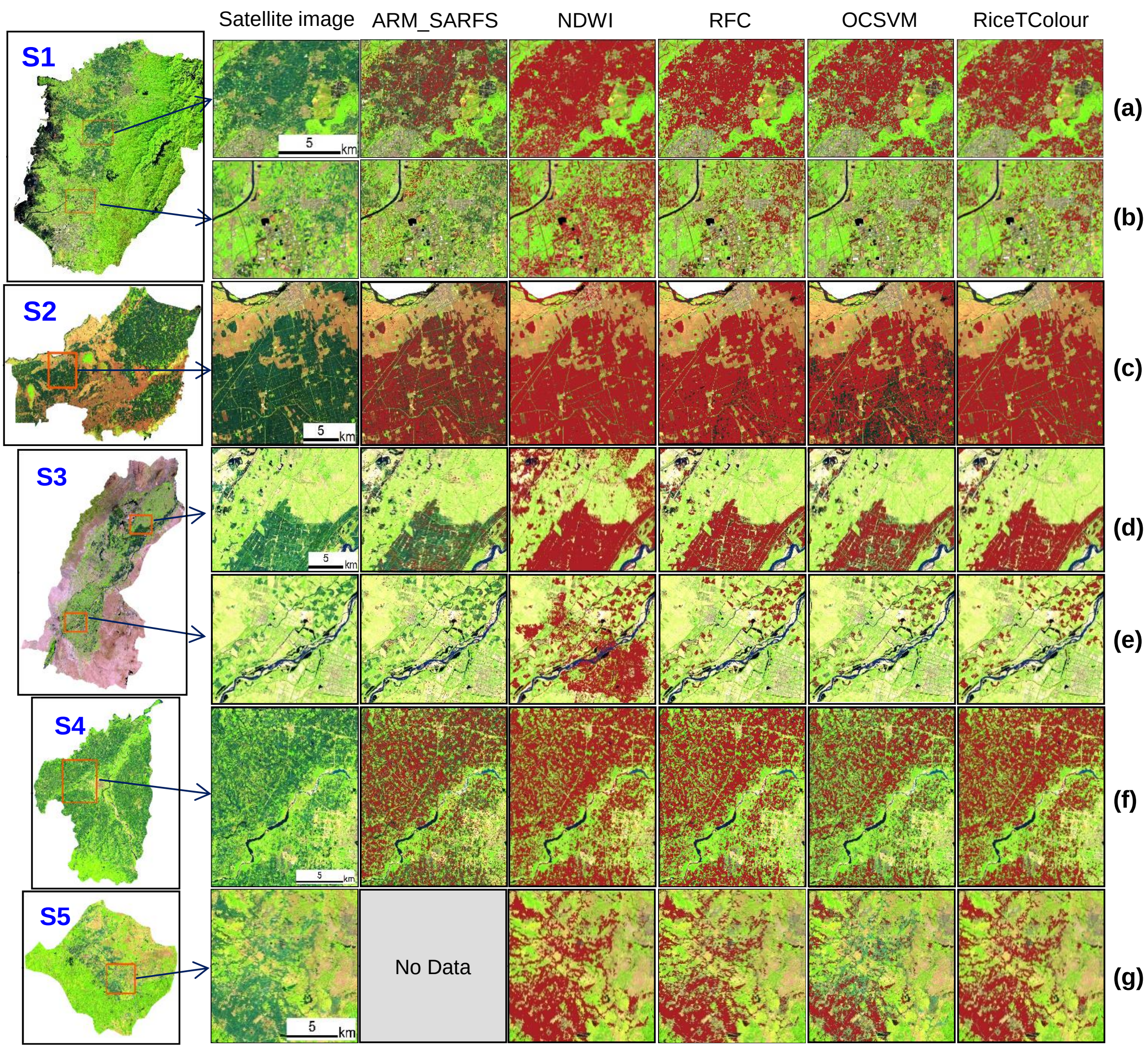

Figure 9. Comparison of paddy rice mapping results achieved by the RiceTColour method and the benchmark methods in the five study sites. Columns from left to right represent the Landsat 8 satellite sensor images, and the results of the ARM-SARFS, NDWI, RFC, OCSVM and the proposed

RiceTColour, respectively. Note that the produced rice maps (in dark red) were overlaid on the satellite images for easy visual interpretation.

Table 4. Accuracies of paddy rice maps generated by the five methods (ARM-SARFS, NDWI, RFC, OCSVM and RiceTColour) in the five study sites. The largest (best) value in each line is highlighted in **bold** font.

Study site		Rice mapping accuracies by different methods				
		ARM-SARFS	NDWI	RFC	OCSVM	RiceTColour
S1	OA (%)	91.13	86.86	95.14	94.31	**97.38**
	PA (%)	42.26	98.14	**98.67**	93.62	92.55
	UA (%)	65.31	45.67	69.87	67.56	**85.09**
	F_1-score	0.52	0.62	0.82	0.78	**0.89**
S2	OA (%)	81.29	96.73	92.46	89.30	**97.23**
	PA (%)	70.97	**98.52**	89.46	77.21	96.51
	UA (%)	81.29	93.58	91.36	94.89	**96.51**
	F_1-score	0.76	0.96	0.90	0.85	**0.97**
S3	OA (%)	92.99	88.98	98.50	98.26	**98.50**
	PA (%)	37.04	**91.01**	86.77	76.72	89.41
	UA (%)	37.04	32.51	86.32	**90.63**	84.50
	F_1-score	0.37	0.48	0.86	0.83	**0.87**
S4	OA (%)	74.65	94.87	96.46	91.54	**96.49**
	PA (%)	60.77	**98.65**	92.95	79.37	96.40
	UA (%)	70.62	89.40	97.94	**98.88**	94.76
	F_1-score	0.65	0.94	0.95	0.88	**0.96**
S5	OA (%)	-	96.70	98.20	94.81	**98.38**
	PA (%)	**-**	**98.86**	95.17	55.97	94.89
	UA (%)	-	76.32	88.39	**90.37**	90.03
	F_1-score	-	0.86	0.92	0.69	**0.92**

Quantitative accuracy assessment further demonstrated the effectiveness and superiority of the proposed method. As shown in Table 4, the RiceTColour method achieved consistently the highest OA compared with the benchmarks across all five study sites, which aligns with the previous visual inspection results (see Fig. 9). Although ARM-SARFS attained moderate overall accuracies (75%-90%) across S1 to S4, it achieved very low producer's accuracies (<71%), particularly in S1 and S3 (only 42.26% and 37.04%, respectively), where the proportion of paddy fields is relatively low (Table 1). NDWI achieved highly accurate PA (91%-99%) over all study areas; however, this was obtained at the cost of high commission error (i.e., low UA). For example, the UA in S3 was only around 33%, indicating that over two-thirds (67%) of the pixels classified as rice were misclassified (i.e., non-rice pixels were erroneously identified as rice pixels). In other words, the area of rice was prominently overestimated, particularly in regions with relatively small proportions of paddy rice (S1, S3 and S5). Both supervised-based classifiers (RFC and OCSVM) acquired promising accuracies (OA and PA) in S1, comparable to those of RiceTColour. However, their producer's accuracies decreased markedly when generalised to S2 to S5. For example, OCSVM achieved a very poor PA, ranging between 55.97% (S5) and 79.37% (S4), when generalised to S2 to S5. In other words, OCSVM failed to detect approximately 20%-45% of the rice fields when applied to unseen imagery. Similarly, the PA of RFC also decreased markedly when generalised to S2 to S5, particularly in S2 (89.46%) and S3 (86.77%). In contrast to the unbalanced benchmarks, the proposed RiceTColour method achieved very high yet balanced rice mapping accuracies not only at the model training site (S1), but also in the generalised areas (S2 to S5). The OA, as well as the PA and UA, exceeded 89% across all five sites (except for UA in S1 and S3). Similarly, the F_1-socre was consistently the highest across all sites, indicating that the RiceTColour method consistently maintained a strong balance between rice identification and misclassification between rice and the other land covers. The superiority of the proposed method can be more intuitively demonstrated using the quantity disagreement and allocation disagreement (Fig. 10). As shown in the figure, RiceTColour achieved a total disagreement (the sum of quantity disagreement and allocation disagreement) below 4% for all five study sites, suggesting a very small difference between the reference data and the generated rice maps. ARM_SARFS and NDWI acquired significantly larger total disagreement than the RiceTColour across the five study sites, with total disagreement exceeding 10% in S2 and S4 for ARM_SARFS and in S1 and S3 for NDWI. Similarly, both supervised classifiers (RFC and OCSVM) were less accurate compared to RiceTColour, particularly in S2, indicating their struggles with unseen imagery.

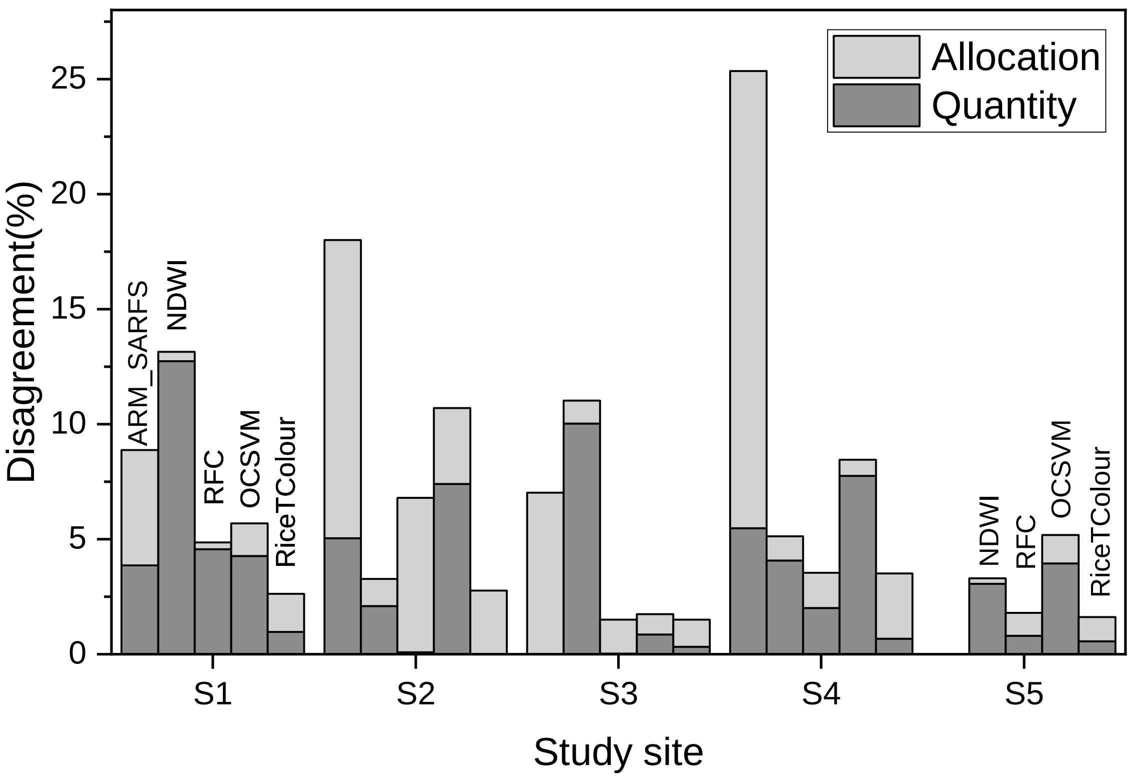

Figure 10. Comparison of the quantity disagreement and allocation disagreement amongst the ARM_SARFS, NDWI, RFC, OCSVM and RiceTColour methods across the five study sites.

5. Discussion

5.1 Mapping transplanted paddy rice fields within original spectral space

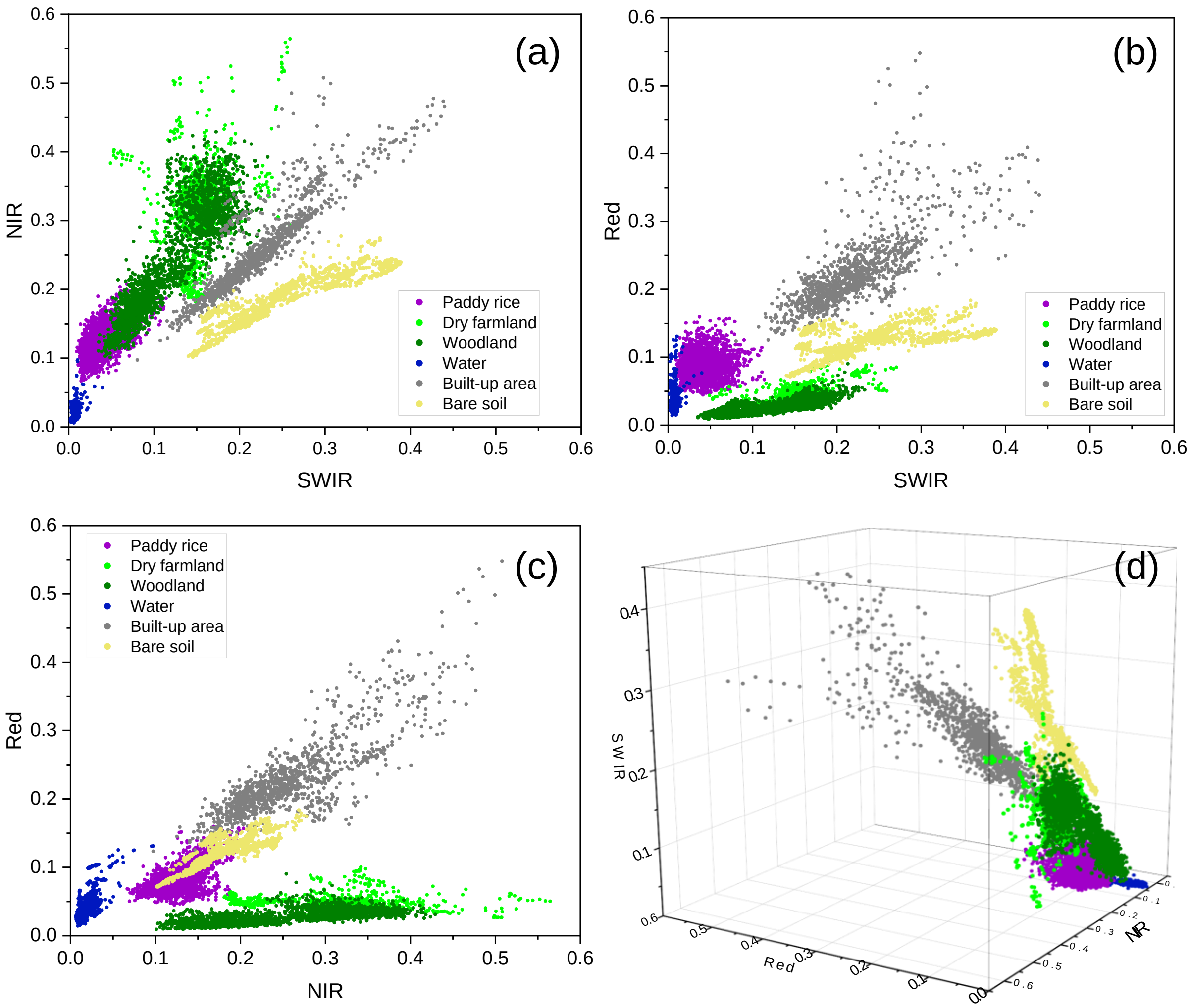

Figure 11. Scatter plots of the training samples for different land covers in the training site (S1) within (a) 2D SWIR-NIR space, (b) 2D SWIR-Red space, (c) 2D NIR-Red space, and (d) 3D SWIR-NIR-Red space.

Paddy rice mapping has long been a significant and persistent challenge in the field of remote sensing because of the substantial spectral overlap between rice and other land covers (e.g., crops, water). We discovered and demonstrated that rice fields exhibit stable and unique spectra (i.e., relatively low values in both SWIR and NIR bands) during the transplanting period in the SWIR and NIR bands (Fig. 5). To investigate whether transplanted paddy rice can be detected directly within original spectral spaces, we illustrated scatter plots of the training samples for different land covers within the 2D spaces and 3D SWIR-NIR-Red space in Fig. 11. As can be seen from the figure, paddy rice was mixed together with other land covers within both the 2D and 3D spectral spaces, especially woodland, dry farmland and water. In other words, it is very challenging to discriminate paddy rice from the other land covers within original spectral space constituted by the SWIR, NIR and Red bands even though unique spectra of paddy rice were seen in them.

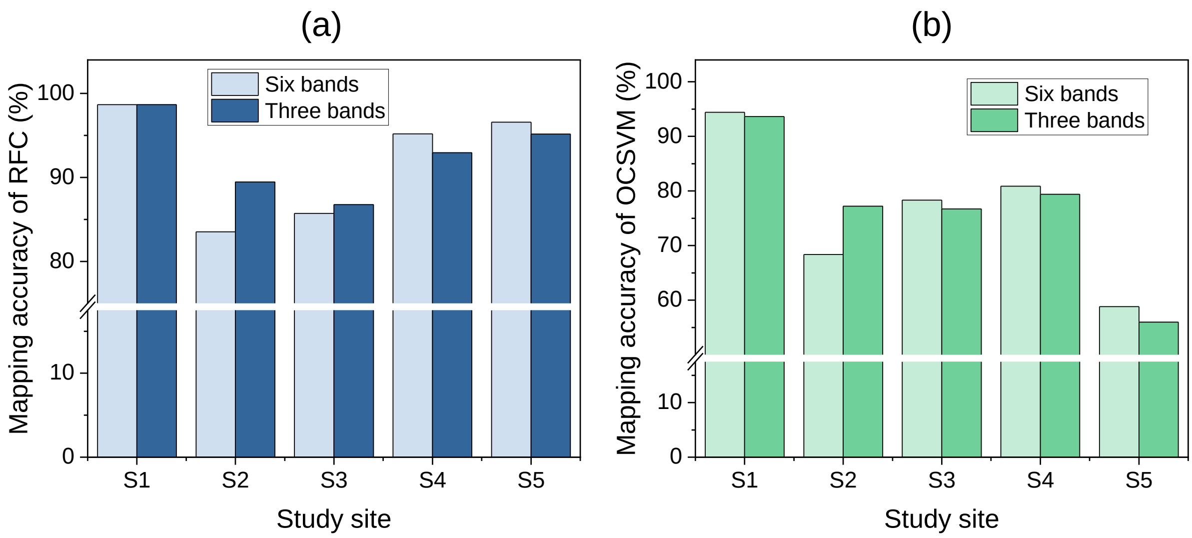

Figure 12. Changes in the accuracy of paddy rice mapping of RFC and OCSVM using different number of spectral bands. Note that 'Three bands' represents SWIR, NIR and Red bands, and 'Six bands' denotes all the six spectral bands of Landsat 8 images.

To investigate whether the number of spectral bands affects the performance of supervised classifiers, we summarised the changes in the accuracy of paddy rice mapping using both RFC and OCSVM with different number of bands in Fig. 12. As can be seen from the figure, both classifiers achieved similarly high mapping accuracies (around 95%) using different numbers of bands in the training site (S1). This indicates that both classifiers can consistently find classification criteria to discriminate paddy rice from other types, regardless of the number of spectral bands used. However, the mapping accuracies of both classifiers decreased significantly when generalising the established classification criteria to unseen data (S2 to S5). This suggests that it is very challenging for both RFC and OCSVM to establish generalisable criteria for detecting paddy rice fields under various environmental conditions, whether in three-band or six-band spectral space.

5.2 Discrimination of transplanted paddy rice fields using the CIE colour space

Differing from commonly used classifier-based, phenology-based and index-based methods, this research proposed an entirely new rice mapping method called RiceTColour, based on the unique spectra (in SWIR and NIR bands) of transplanted rice fields using the CIE colour space. By transforming the SWIR, NIR and Red bands into the CIE colour space, the scatterplots of the training samples for different land covers within the CIE coordinate system and the corresponding satellite sensor image are generated and demonstrated in Fig. 13 (a). As depicted by the figure, paddy rice, represented by unique dark colours (the right column of Fig. 13 (a)), can be readily distinguished from the other land covers in the novel false-colour imagery composed of the SWIR (R), NIR (G) and Red (B) bands. More importantly, as mentioned in the methodology section, paddy rice occupies specific, exclusive areas within the 2-D CIE space, with very little overlap with the other land covers, suggesting that paddy rice can be easily discriminated from them (the left column of Fig. 13 (a)). The SWIR band that has been reported widely to be sensitive to soil moisture (Xiao et al., 2006; Wang et al., 2007; Tian et al., 2015) was used as the red channel. The converted x value in the CIE coordinate system, therefore, signifies the strength of dryness (the lower the SWIR value, the higher the water content) (Eq. (2) and Fig. 13 (a)). Paddy rice and water with low SWIR values acquired relatively low x values (below 0.35) in the CIE coordinate system, making them being distributed in the green and blue gamut. The NIR band, positioned within the visible-light absorption area (where chlorophyll in plant leaves absorbs visible light) and sensitive to vegetation greenness, was used as the green channel. Thus, the converted y values of paddy rice with rice seedlings (generally exceeding 0.35) are higher than those of water, refining paddy rice being located in the green gamut. This explains why transplanted rice fields locate in unique regions in the CIE colour space, and exhibit corresponding unique colours in the false-colour imagery composited using these three bands Fig. 13 (a).

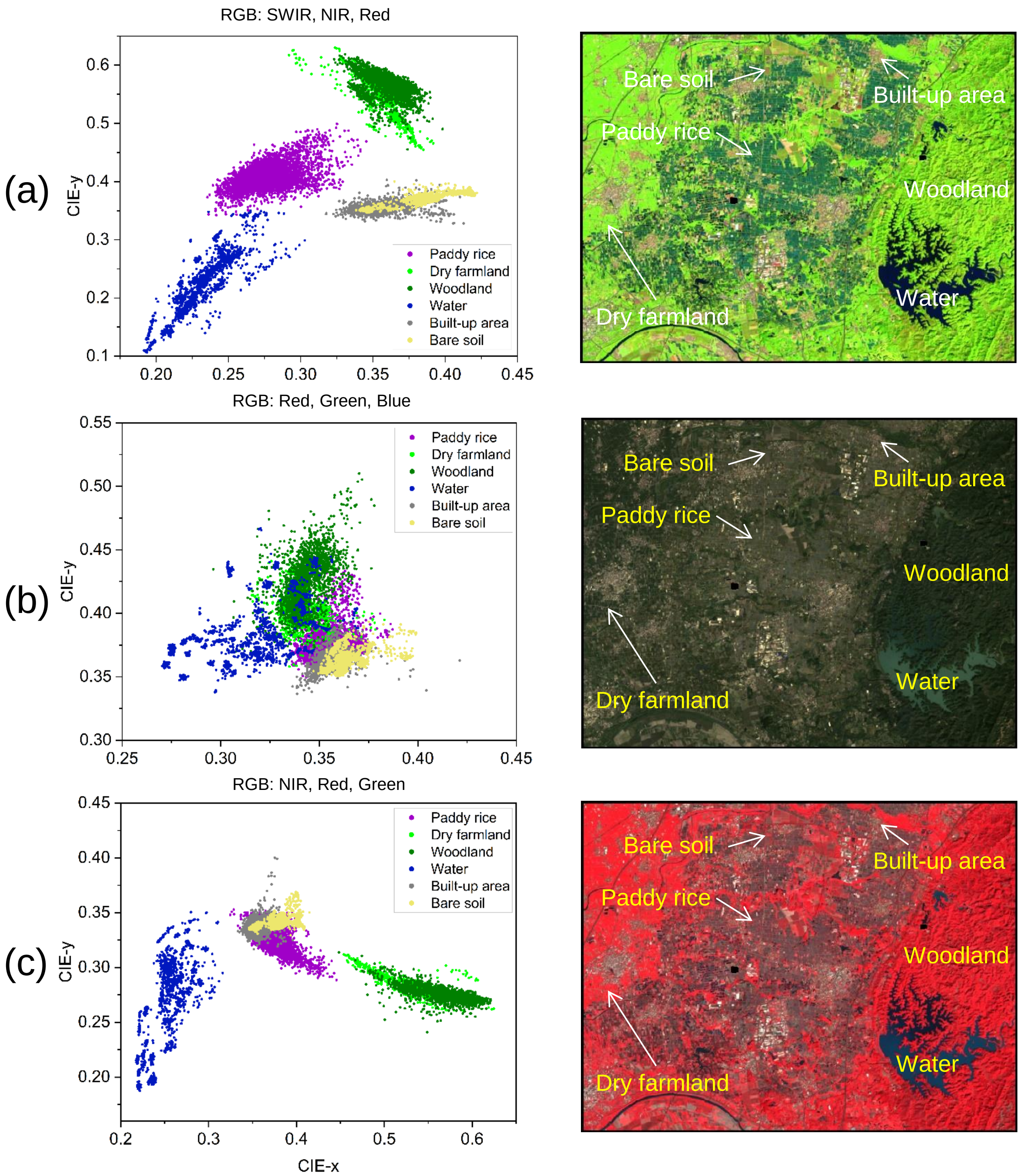

Figure 13. Scatterplots of the training samples within the CIE colour space (left column) in the training site (S1) using different band combinations and their corresponding satellite sensor images (right

column). (a) False-colour imagery composited using the SWIR, NIR and Red bands, (b) true-colour imagery, and (c) false-colour imagery using the NIR, Red and Green bands. Typical land covers are marked and labelled in the satellite sensor images.

To make a comparison, we also demonstrate the scatterplots of the training samples within the CIE colour space using the other two types of imagery: the true-colour imagery using the Red, Green and Blue bands (Fig. 13 (b)) and the conventional false-colour imagery using the NIR, Red and Green bands (Fig. 13 (c)). To facilitate visual interpretation, typical land covers were marked and labelled on the imagery. For each image, we also demonstrated the corresponding satellite sensor images composited with different bands (see the right column of Fig. 13). For the true-colour imagery, the land covers were found to overlap each other within the CIE space (the left column of Fig. 13 (b)). Accordingly, it is very challenging to visually differentiate one land cover from another in the satellite sensor image (the right column of Fig. 13 (b)). Similarly, paddy rice, built-up area and bare soil were mixed together within the CIE space using the conventional false-colour imagery (the left column of Fig. 13 (c)). As expected, it is almost impossible to discern paddy rice from built-up area and bare soil since they exhibit similar gray colours in the imagery (the right column of Fig. 13 (c)). It is evident from the above analysis that if a certain land cover can be visually discriminated from the others in the imagery, it can also be readily differentiated within the CIE colour space.

5.3 Transferability of RiceTColour

While RiceTColour was established based on the training samples collected in S1, it achieved surprisingly high (above 95%) and relatively stable (OA ranging between 95.76% and 98.50%) mapping accuracies across all five study sites (including the generalised four sites S2 to S5), as shown by Table 4 and Fig. 10. In other words, the proposed RiceTColour method possesses strong transferability for rice mapping, which can be primarily attributed to two reasons:

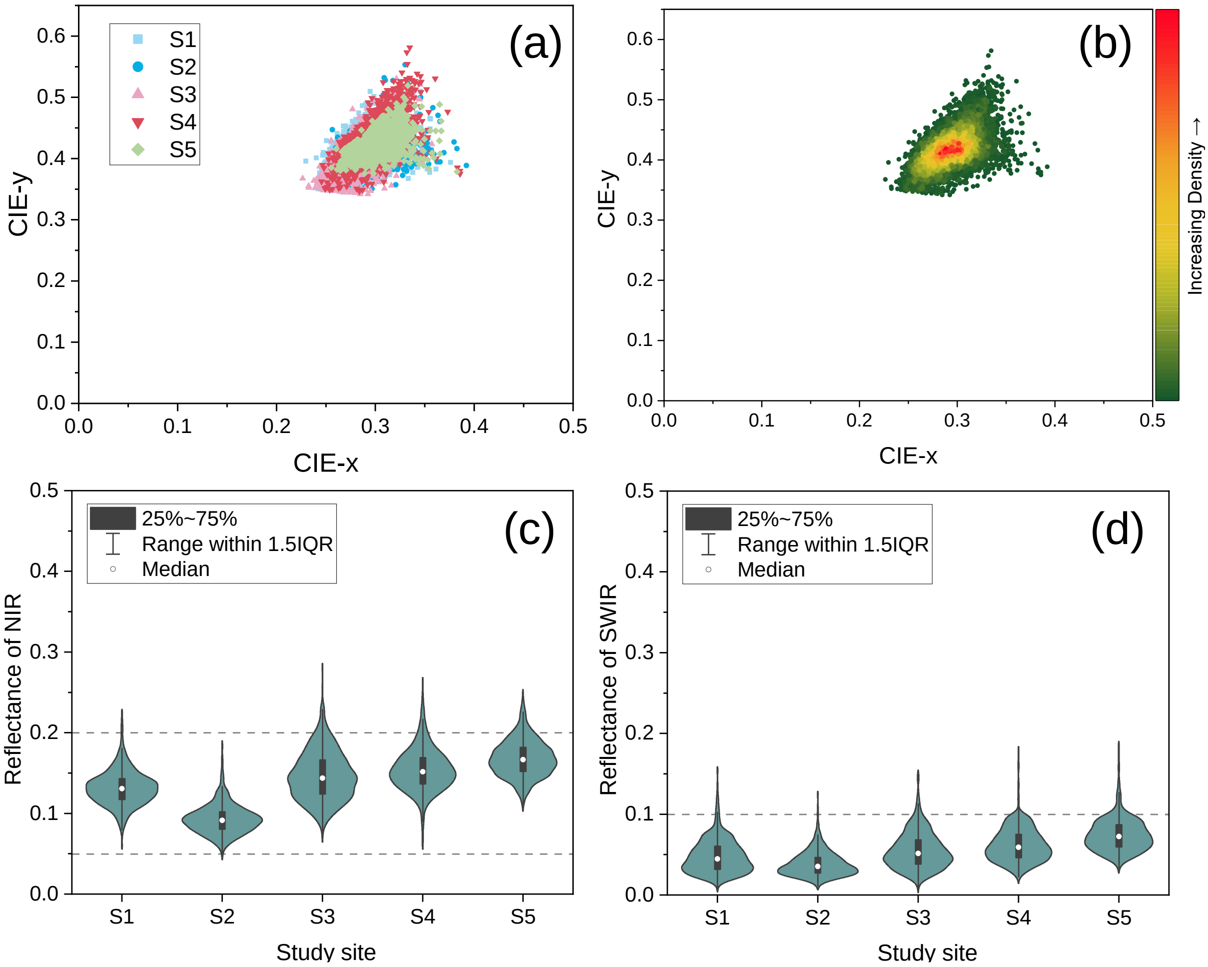

Figure 14. (a) Scatterplots of the validation samples for paddy rice across the five sites within the CIE colour space. (b) Point density of all the validations samples in the five sites within the CIE colour space. Changes in spectral features for the corresponding NIR (c) and SWIR (d) bands.

First, the distinctive physical feature of rice is its exclusive cultivation in flooded soils (Xiao et al., 2005), which creates a unique mixed soil-water-rice environment during the transplanting period. Such a unique and exclusive environment remains consistent across various rice-planting regions, as evidenced by the consistently dark green colour of paddy rice in all five study areas shown in Fig. 6. We, therefore, speculate that samples of transplanted paddy rice fields from different geographical regions should fall in similar areas within the CIE colour space because of their similar spectra (colours). To validate this hypothesis, we created the scatterplots of the validation samples for paddy rice across the five sites within the CIE colour space (Fig. 14 (a) and (b)). Besides, we also demonstrated the changes in the spectral values for the corresponding NIR and SWIR bands of these samples (Fig. 14 (c) and (d)). As expected, the samples from different study areas are concentrated together in the CIE chromaticity coordinates, with only a very few points distributed outside the main cluster (Fig. 14 (a)). As shown by the point density map (Fig. 14 (b)), the samples are primarily located in an area with CIE-*x* values varying between 0.24-0.34 and CIE-*y* values ranging from 0.35 to 0.48 in the CIE chromaticity coordinates. This benefits from the stable and unique spectral features of transplanted paddy rice in the NIR and SWIR bands. As shown in Fig. 14 (c) and (d), the variations in both bands are relatively small across all five sites, with NIR ranging from 0.05 to 0.20 and SWIR varying between 0 and 0.10. In summary, with similar spectra in NIR and SWIR bands, transplanted rice fields fall in similar areas within the CIE colour space regardless of geographical region, which is the fundamental reason for the strong robustness and transferability of our method.

Second, the proposed RiceTColour method is a completely parameter-free rice mapping method. The established classification criteria (Eq. (4)) in this research can, therefore, be adopted directly by users for rice mapping in other regions (like S2 to S5 in our experiments), which avoids complicated and tedious parameter-tuning work. In contrast, existing methods rely heavily on parameter (hyperparameter) settings for accurate rice mapping, which is responsible for their relatively weak transferability. For example, several previous efforts have illustrated that rice mapping results were strongly influenced by the key parameters of supervised classifiers (e.g., the gamma and penalty parameters for SVM) (Sonobe et al., 2014; Son et al., 2018; Ni et al., 2021). Similarly, phenology-based methods with a set of rules (Torbick et al., 2011; Dong et al., 2015; Xia et al., 2021; Zhan et al., 2021), as well as index-based methods (Boschetti et al., 2014; Xu et al., 2023), generally require several parameters (thresholds) to be determined for rice mapping. It is widely acknowledged that the process of parameter tuning is technologically-challenging, physically arduous, and time-intensive

(Zhang and Zhang, 2022). Further, the recommended optimal parameters are essentially only optimal locally and usually vary significantly between different regions (Dong et al., 2016; Xu et al., 2023). This results in a lack of generalisability for existing methods, as demonstrated by the supervised classifier (RFC and OCSVM) in this research (see Table 4 and Fig. 10).

5.4 Applicable conditions of RiceTColour at large scales

With the availability of a large volume of remotely sensed imagery and the rapid development of online efficient satellite sensor image processing platforms (such as GEE), there is an emerging trend for mapping paddy rice at large scales, such as the national, hemispheric or even global scales (e.g., Xiao et al., 2005; Dong et al., 2016; Carrasco et al., 2022; Han et al., 2022). This poses new requirements for paddy rice mapping and classification methods, which should be accurate, efficient and transferable. Moreover, methods are expected to utilise as few images as possible since the greater the volume of used imagery, the more challenging the data collection, which is a primary obstacle to large-scale mapping (Dong and Xiao, 2016). Obviously, the proposed straightforward, parameter-free and transferable RiceTColour method fully satisfies the requirements regarding efficiency and transferability. Furthermore, instead of requiring a full year (or full growing season) image time-series like the classifier-based and phenology-based methods (Kontgis et al., 2015; Dong et al., 2016; Cao et al., 2021; Ni et al., 2021; Carrasco et al., 2022), the proposed RiceTColour method utilises only images collected during rice transplanting, which is especially beneficial for rice mapping over large scales.

While the developed method is evidently suitable for large-scale mapping given its unique advantages, some precautions should be taken into account as they might affect the generalisation of the method. First, while the transplanting-based RiceTColour method removes the requirement for full year (or full growing season) time-series images, the relatively short time period of transplanting might result in a lack of available imagery in certain regions due to cloud contamination, especially for those optical satellite sensors with long revisit cycles, such as the Landsat series. For example, in our experiments, a total of 14, 15 and 10 satellite sensor observations were available for S1, S2 and S4 during the transplanting period, but only 3, 8 and 4 of these observations were deemed valid (with cloud cover < 20%), respectively. In fact, in addition to transplanting, the preceding flooding, characterised by flooded soil, or open water yet not transplanted (or planted) rice seedlings, represents another unique period for paddy rice (Dong et al., 2015; Zhan et al., 2021). Future research should explore the possibility of including the flooding period in RiceTColour, which could broaden the applicability of the proposed method to a wider time period. Second, since the proposed method is established based on the spectra of Landsat 8 imagery, its rice detection capability might be affected if other optical images, such as Sentinel-2, are used as the data source. This is because the optical sensors generally differ in spectral bandwidth and spectral response function (Shang and Zhu, 2019). Therefore, spectral harmonization is needed to ensure multi-sensor spectral consistency when generalising the proposed method to other types of optical imagery. Third, since the proposed RiceTColour is designed to detect the mixed soil-water-rice environment for rice mapping, it could potentially misclassify wetlands and regions surrounding water bodies (e.g., lakeshore and riverside areas) as paddy rice (Xiao et al., 2005), as these areas often consist of soil, water and grass during the rice transplanting period. Future research may seek to incorporate images collected at other phenological stages to the proposed method to further refine the classification of paddy rice based on phenological differences between human-managed paddy rice and natural grass (Zhou et al., 2016). It should also be noted that the proposed method might not be applicable for detecting direct-seeded rice fields where rice grows in moist soil with a small amount of water (Sah et al., 2023), rather than flooded soil as in transplanted rice fields. Fourth, since RiceTColour relies on imagery collected during transplanting, it is necessary to obtain access to crop calendar information to determine the transplanting period. Such information might not be readily available to users who are not familiar with a given study area. Besides, cropping calendars may vary greatly across large areas owing to variation in climate, terrain conditions, irrigation schemes and farmer's management practices (Laborte et al., 2017; Mishra et al., 2021). Under such circumstances, it would be better to adopt composite images (such as S1, S2 and S4 in our experiments) for rice detection, as some paddy fields where transplanting has not yet occurred might be omitted when using single images. Besides, users should seek to incorporate the proposed method with algorithms capable of detecting crop calendars automatically for paddy rice mapping over large areas (e.g., Zhang et al., 2015; Dong et al., 2016).

5.5 Final Remarks

The CIE colour space has been adopted within the remote sensing community for mapping and classification tasks. However, this is primarily in the research field of water colour remote sensing (Pitarch et al., 2019), with applications generally classified into two groups: water colour mapping (Wang et al., 2015; Shen et al., 2019) and algal bloom detection (e.g., Liu et al., 2022; Dai et al., 2023). Only a few studies have introduced the CIE space in land remote sensing (Silva et al., 2018). This can be attributed mainly to the relatively simple composition of categories in the water environment, compared to much more complex compositions on land. To the best of our knowledge, this is the first effort to employ the CIE space for crop mapping. Traditional feature space analysis across various spectral bands has been adopted for remote sensing of various land surface variables (e.g., soil moisture) by establishing mathematical formulations representing the relationships between distributions in feature space (Zhan et al., 2007; Cai et al., 2023). However, it can be challenging to identify classification rules within spectral feature space due to the complexity of the land environment. This complexity often means that distributions representing different land covers overlap in feature space, as demonstrated in Fig. 11 of this research, and in previous studies (Zhan et al., 2007; Cai et al., 2023). By transforming the spectra from the traditional feature space to the CIE colour space, we observed that paddy rice fields with unique spectra (colours) can be readily discriminated from other land covers (Fig. 7), indicating the superiority of the CIE space over feature space for land cover mapping. We further demonstrated that the CIE space has the potential to discriminate certain land categories if they present unique colours (spectra) in remotely sensed imagery. This finding opens up new avenues for land cover mapping and classification.

SAR data have received increasing attention from researchers for developing rice detection methods (Dong and Xiao, 2016; Zhan et al., 2021; Xu et al., 2023). This is primarily because the acquisition of SAR data is not affected by weather conditions (Dong and Xiao, 2016). However, in this research, the proposed optical imagery-based method was found to be significantly more accurate than the SAR-based methods, primarily due to its two advantages. First, the parameter-free RiceTColour method avoids the complex and tedious parameter tuning work, making it perform relatively stably across different regions. In contrast, SAR-based methods typically involve a large number of sensitive parameters that usually need to be adjusted in different regions (Zhan et al., 2021), which may affect significantly their mapping capability. Second, the proposed method is established based on optical remotely sensed imagery, thereby, avoiding heavy salt-and-pepper noise, as observed in the classified maps generated by the SAR-based methods in our experiments (Fig. 9). Despite this, SAR data can serve as a substitute in regions with concentrated paddy rice (e.g., S2 and S4 in this paper) when optical data during the transplanting period are not available. SAR data are not suggested to be applied to regions with scattered paddy rice (e.g., S1 and S3 in this paper), where over half of the rice fields were omitted according to our experiments.

5. Conclusions

As the only crop grown in flooded soil, paddy rice experiences a unique growing environment (i.e., mixture of soil, water and rice seedlings) during the transplanting period, which provides excellent opportunities for identifying paddy rice from other land covers. In this paper, an entirely new method, called RiceTColour, was proposed for detecting paddy rice according to its unique spectra during the period of rice transplanting as observed in remotely sensed imagery. We discovered and demonstrated for the first time that transplanted rice fields consistently exhibit distinctive spectra in the SWIR and NIR bands, irrespective of geographical location. Based on this critical finding, the two spectral bands with the Red band were transformed into the 2-D CIE colour space, where paddy rice was found to occupy specific regions (representing unique colours) that can be readily and completely separated from other land covers. Straightforward, but specific classification criteria were, therefore, established within the CIE colour space to differentiate paddy rice from the other land covers. The proposed RiceTColour method represents a new paradigm for paddy rice mapping, established upon the previous underexplored unique spectra of transplanted paddy fields exhibited in remotely sensed imagery using the CIE colour space.

In total, five rice-planting regions distributed across different geographical regions, characterised by different climates, rice cropping intensities, irrigation schemes and cultural practices, were selected to investigate the effectiveness and transferability of the proposed method. Experimental results demonstrated that the RiceTColour method consistently achieved the most accurate and balanced classifications compared with the benchmark comparators across all five sites. In particular, RiceTColour performed relatively stably, producing an overall accuracy exceeding 95% in the training site (S1), as well as the four testing-only sites (S2 to S5), which is an encouraging and impressive result. Such efficient yet stable rice mapping results across various rice-planting regions suggest the strong generalisation capability of the proposed parameter-free and efficient RiceTColour method. Paddy rice accounts for approximately 12% of global cropland area, and is an important staple crop feeding approximately half of the world’s population. Mapping paddy rice is, thus, a key requirement in ensuring global food security. The proposed efficient, robust and generalisable

RiceTColour method holds great potential for widespread application in various rice-planting areas worldwide.

Acknowledgements

This research was funded jointly by the National Key Research and Development Program of China (2021YFD1500100), the Strategic Priority Research Program of the Chinese Academy of Sciences (Grant No. XDA28070500), the Jilin Scientific and Technological Development Program (20220201158GX), the Capital Construction Fund of Jilin Province (2021C045-2), and the Common Application Support Platform for National Civil Space Infrastructure Land Observation Satellites (Grant No. 2017-000052-73-01-001735).

References

Ashourloo, D., Shahrabi, H.S., Azadbakht, M., Aghighi, H., Nematollahi, H., Alimohammadi, A., Matkan, A.A., 2019. Automatic canola mapping using time series of sentinel 2 images. ISPRS J. Photogramm. Remote Sens. 156, 63-76.

Beck, H.E., Zimmermann, N.E., McVicar, T.R., Vergopolan, N., Berg, A., Wood, E.F., 2018. Present and future Koppen-Geiger climate classification maps at 1-km resolution. Sci. Data. 5, 180214.

Belgiu, M., Dragut, L., 2016. Random forests in remote sensing: a review of applications and future directions. ISPRS J. Photogramm. Remote Sens. 114, 24–31.

Boschetti, M., Nutini, F., Manfron, G., Brivio, P.A., Nelson, A., 2014. Comparative analysis of normalised difference spectral indices derived from MODIS for detecting surface water in flooded rice cropping systems. PloS One. 9, e88741.

Bouman, B., 2009. How much water does rice use. Management. 69, 115-133.

Breiman, L., 2001. Random forests. Mach. Learn. 45, 5-32.

Bridhikitti, A., Overcamp, T.J., 2012. Estimation of Southeast Asian rice paddy areas with different ecosystems from moderate-resolution satellite imagery. Agr. Ecosyst. Environ. 146, 113-120.

C.I.E, 1932. Commission Internationale de l'Eclairage Proceedings 1931. Cambridge Univ. Press, pp. 19-29.

Cai, J., Yu, W.Y., Fang, Q., Zi, R.Y., Fang, F.Y., Zhao, L.S., 2023. Extraction of Rocky Desertification Information in the Karst Area Based on the Red-NIR-SWIR Spectral Feature Space. Remote Sens. 15, 3056.

Cao, J.J., Cai, X.L., Tan, J.W., Cui, Y.L., Xie, H.W., Liu, F.P., Yang, L., Luo, Y.F., 2021. Mapping paddy rice using Landsat time series data in the Ganfu Plain irrigation system, Southern China, from 1988-2017. Int. J. Remote Sens. 42, 1556-1576.

Carrasco, L., Fujita, G., Kito, K., Miyashita, T., 2022. Historical mapping of rice fields in Japan using phenology and temporally aggregated Landsat images in Google Earth Engine. ISPRS J. Photogramm. Remote Sens. 191, 277-289.

Chen, C., McNairn, H., 2006. A neural network integrated approach for rice crop monitoring. Int. J. Remote Sens. 27, 1367-1393.

Chen, H., Li, H., Liu, Z., Zhang, C., Zhang, S., Atkinson, P.M., 2023. A novel Greenness and Water Content Composite Index (GWCCI) for soybean mapping from single remotely sensed multispectral images. Remote Sens. Environ. 295, 113679.

Chen, H., Meng, F., Yu, Z.N., Tan, Y.Z., 2022. Spatial-temporal characteristics and influencing factors of farmland expansion in different agricultural regions of Heilongjiang Province, China. Land Use Policy, 115, 106007.

Chen, Y., Zhao, X., Jia, X., 2015. Spectral–Spatial Classification of Hyperspectral Data Based on Deep Belief Network. IEEE J. Sel. Top. Appl. Earth Obs. Remote Sens. 8, 2381-2392.

Clauss, K., Yan, H., Kuenzer, C., 2016. Mapping paddy rice in China in 2002, 2005, 2010 and 2014 with MODIS time series. Remote Sens. 8, 434.

Dai, Y.H., Yang, S.B., Zhao, D., Hu, C.M., Xu, W., Anderson, D.M., Li, Y., Song, X.P., Boyce, D.G., Gibson, L., Zheng, C.M., Feng, L., 2023. Coastal phytoplankton blooms expand and intensify in the 21st century. Nature, 615, 280-284.

Dong, J., Xiao, X., 2016. Evolution of regional to global paddy rice mapping methods: A review. ISPRS J. Photogramm. Remote Sens. 119, 214-227.

Dong, J., Xiao, X., Kou, W., Qin, Y., Zhang, G., Li, L., Jin, C., Zhou, Y., Wang, J., Biradar, C., Liu, J., Moore, B., 2015. Tracking the dynamics of paddy rice planting area in 1986–2010 through time series Landsat images and phenology-based algorithms. Remote Sens. Environ. 160, 99-113.

Dong, J., Xiao, X., Menarguez, M.A., Zhang, G., Qin, Y., Thau, D., Biradar, C., Moore III, B., 2016. Mapping paddy rice planting area in northeastern Asia with Landsat 8 images, phenology-based algorithm and Google Earth Engine. Remote Sens. Environ. 185, 142-154.

FAO. 2022. World Food and Agriculture – Statistical Yearbook 2022. Rome. https://doi.org/10.4060 /cc2211en.

Foody, G.M., 2021. Impacts of ignorance on the accuracy of image classification and thematic mapping. Remote Sens. Environ. 259, 112367.

Han, J., Zhang, Z., Luo, Y., Cao, J., Zhang, L., Zhuang, H., Cheng, F., Zhang, J., Tao, F., 2022. Annual paddy rice planting area and cropping intensity datasets and their dynamics in the Asian monsoon region from 2000 to 2020. Agric. Syst. 200, 103437.

Heiskanen, J., 2006. Estimating aboveground tree biomass and leaf area index in a mountain birch forest using ASTER satellite data. Int. J. Remote Sens. 27, 1135-1158.

Huang, W.R., Liu, P.Y., Hsu, J., 2021. Multiple timescale assessment of wet season precipitation estimation over Taiwan using the PERSIANN family products. Int. J. Appl. Earth Obs. Geoinf. 103, 102521.

Jarchow, C.J., Nagler, P.L., Glenn, E.P., 2017. Greenup and evapotranspiration following the Minute 319 pulse flow to Mexico: An analysis using Landsat 8 Normalized Difference Vegetation Index (NDVI) data. Ecol. Eng. 106, 776-783.

Ji, L., Zhang, L., Wylie, B., 2009. Analysis of Dynamic Thresholds for the Normalized Difference Water Index. Photogramm. Eng. Remote Sensing, 75, 1307-1317.

Kontgis, C., Schneider, A., Ozdogan, M., 2015. Mapping rice paddy extent and intensification in the Vietnamese Mekong River Delta with dense time stacks of Landsat data. Remote Sens. Environ. 169, 255-269.

Krizhevsky, A., Sutskever, I., Hinton, G.E., 2012. ImageNet classification with deep Convolutional Neural Networks. In: NIPS2012: Neural Information Processing Systems. Lake Tahoe, Nevada, pp. 1–9.

Laborte, A.G., Gutierrez, M.A., Balanza, J.G., Saito, K., Zwart, S.J., Boschetti, M., Murty, M.V.R., Villano, L., Aunario, J.K., Reinke, R., Koo, J., Hijmans, R.J., Nelson, A., 2017. RiceAtlas, a spatial database of global rice calendars and production. Scientific Data, 4, 170074.

LeCun, Y., Bengio, Y., Hinton, G., 2015. Deep learning. Nature, 521, 436-444.

LeToan, T., Ribbes, F., Wang, L.F., Floury, N., Ding, K.H., Kong, J.A., Fujita, M., Kurosu, T., 1997. Rice crop mapping and monitoring using ERS-1 data based on experiment and modeling results. IEEE Trans. Geosci. Remote Sens. 35, 41-56.

Liu, R.J., Xiao, Y.F., Ma, Y., Cui, T.W., An, J.B., 2022. Red tide detection based on high spatial resolution broad band optical satellite data. ISPRS J. Photogramm. Remote Sens. 184, 131-

147.

Lu, D., Weng, Q., 2007. A survey of image classification methods and techniques for improving classification performance. Int. J. Remote Sens. 28, 823-870.

Luintel, N., Ma, W., Ma, Y., Wang, B., Xu, J., Dawadi, B., Mishra, B., 2021. Tracking the dynamics of paddy rice cultivation practice through MODIS time series and PhenoRice algorithm. Agric. For. Meteorol. 307, 108538.

Maiti, A., Acharya, P., Sannigrahi, S., Zhang, Q., Bar, S., Chakraborti, S., Gayen, B.K., Barik, G., Ghosh, S., Punia, M., 2022. Mapping active paddy rice area over monsoon asia using time-series Sentinel-2 images in Google earth engine; a case study over lower gangetic plain. Geocarto Int. 37, 10254-10277.

McCloy, K.R., Smith, F.R., Robinson, M.R., 1987. MONITORING RICE AREAS USING LANDSAT MSS DATA. Int. J. Remote Sens. 8, 741-749.

Mishra, B., Busetto, L., Boschetti, M., Laborte, A., Nelson, A., 2021. RICA: A rice crop calendar for Asia based on MODIS multi year data. Int. J. Appl. Earth Obs. Geoinf. 103, 102471.

Ni, R., Tian, J., Li, X., Yin, D., Li, J., Gong, H., Zhang, J., Zhu, L., Wu, D., 2021. An enhanced pixel-based phenological feature for accurate paddy rice mapping with Sentinel-2 imagery in Google Earth Engine. ISPRS J. Photogramm. Remote Sens. 178, 282-296.

Nogueira, K., Penatti, O.A.B., dos Santos, J.A., 2017. Towards better exploiting convolutional neural networks for remote sensing scene classification. Pattern Recognit. 61, 539-556.

Onojeghuo, A.O., Blackburn, G.A., Wang, Q., Atkinson, P.M., Kindred, D., Miao, Y., 2018. Mapping paddy rice fields by applying machine learning algorithms to multi-temporal Sentinel-1A and Landsat data. Int. J. Remote Sens. 39, 1042-1067.

Panigrahy, S., Parihar, J.S., 1992. Role of middle infrared bands of Landsat thematic mapper in determining the classification accuracy of rice. Int. J. Remote Sens.13, 2943-2949.

Patra, S.K., Shekher, M., Solanki, S.S., Ramachandran, R., Krishnan, R., 2006. A technique for generating natural colour images from false colour composite images. Int. J. Remote Sens. 27, 2977-2989.

Peng, D., Huete, A.R., Huang, J., Wang, F., Sun, H., 2011. Detection and estimation of mixed paddy rice cropping patterns with MODIS data. Int. J. Appl. Earth Obs. Geoinf. 13, 13-23.

Pitarch, J., van der Woerd, H.J., Brewin, R.J.W., Zielinski, O., 2019. Optical properties of Forel-Ule water types deduced from 15 years of global satellite ocean color observations. Remote Sens. Environ. 231, 111249.

Pontius, R.G., Millones, M., 2011. Death to Kappa: birth of quantity disagreement and allocation disagreement for accuracy assessment. Int. J. Remote Sens. 32, 4407-4429.

Qin, Y., Xiao, X., Dong, J., Zhou, Y., Zhu, Z., Zhang, G., Du, G., Jin, C., Kou, W., Wang, J., Li, X., 2015. Mapping paddy rice planting area in cold temperate climate region through analysis of time series Landsat 8 (OLI), Landsat 7 (ETM+) and MODIS imagery. ISPRS J. Photogramm. Remote Sens. 105, 220-233.

Qiu, S., Zhu, Z., Woodcock, C.E., 2020. Cirrus clouds that adversely affect Landsat 8 images: What are they and how to detect them? Remote Sens. Environ. 246, 111884.

Rad, A.M., Ashourloo, D., Shahrabi, H.S., Nematollahi, H., 2019. Developing an Automatic Phenology-Based Algorithm for Rice Detection Using Sentinel-2 Time-Series Data. IEEE J. Sel. Top. Appl. Earth Obs. Remote Sens. 12, 1471-1481.

Sah, S., Haldar, D., Chandra, S., Nain, A.S., 2023. Discrimination and monitoring of rice cultural types using dense time series of Sentinel-1 SAR data. Ecol. Inform. 76, 102136.

Sakamoto, T., Van Phung, C., Kotera, A., Nguyen, K.D., Yokozawa, M., 2009. Analysis of rapid expansion of inland aquaculture and triple rice-cropping areas in a coastal area of the Vietnamese Mekong Delta using MODIS time-series imagery. Landsc. Urban Plan. 92, 34-46.

Saunois, M., Stavert, A.R., Poulter, B., Bousquet, P., Canadell, J.G., Jackson, R.B., Raymond, P.A., Dlugokencky, E.J., Houweling, S., Patra, P.K., et al., 2020. The Global Methane Budget 2000-2017. Earth Syst. Sci. Data 12, 1561-1623.

Sayler, K., 2020. Landsat 8 Collection 1 (C1) Land Surface Reflectance Code (LaSRC) Product Guide. Retrieved from https://prd-wret.s3.us-west-2.amazonaws.com/assets/palladium/production/atoms/files/LSDS-1368_L8_C1-LandSurfaceReflectanceCode-LASRC_Product Guide-v3.pdf

Schölkopf, B., Platt, J.C., Shawe-Taylor, J., Smola, A.J., Williamson, R.C., 2001. Estimating the support of a high-dimensional distribution. Neural Comput. 13, 1443-1471.

Shang, R., Zhu, Z., 2019. Harmonizing Landsat 8 and Sentinel-2: A time-series-based reflectance adjustment approach. Remote Sens. Environ. 235, 111439.

Shao, Y., Fan, X., Liu, H., Xiao, J., Ross, S., Brisco, B., Brown, R., Staples, G., 2001. Rice monitoring and production estimation using multitemporal RADARSAT. Remote Sens. Environ. 76, 310-325.

Shen, Q., Yao, Y., Li, J.S., Zhang, F.F., Wang, S.L., Wu, Y.H., Ye, H.P., Zhang, B., 2019. A CIE Color Purity Algorithm to Detect Black and Odorous Water in Urban Rivers Using High-Resolution Multispectral Remote Sensing Images. IEEE Trans. Geosci. Remote Sens. 57, 6577-6590.

Silva, G.F., Carneiro, G.B., Doth, R., Amaral, L.A., de Azevedo, D.F.G., 2018. Near real-time shadow detection and removal in aerial motion imagery application. ISPRS J. Photogramm.

Remote Sens. 140, 104-121.

Son, N.T., Chen, C.F., Chen, C.R., Minh, V.Q., 2018. Assessment of Sentinel-1A data for rice crop classification using random forests and support vector machines. Geocarto Int. 33, 587-601.

Son, N.-T., Chen, C.-F., Chen, C.-R., Toscano, P., Cheng, Y.-S., Guo, H.-Y., Syu, C.-H., 2021. A phenological object-based approach for rice crop classification using time-series Sentinel-1 Synthetic Aperture Radar (SAR) data in Taiwan. Int. J. Remote Sens. 42, 2722-2739.

Sonobe, R., Tani, H., Wang, X.F., Kobayashi, N., Shimamura, H., 2014. Parameter tuning in the support vector machine and random forest and their performances in cross- and same-year crop classification using TerraSAR-X. Int. J. Remote Sens. 35, 7898-7909.

Stehman, S.V., Foody, G.M., 2019. Key issues in rigorous accuracy assessment of land cover products. Remote Sens. Environ. 231, 111199.

Stroppiana, D., Boschetti, M., Azar, R., Barbieri, M., Collivignarelli, F., Gatti, L., Fontanelli, G., Busetto, L., Holecz, F., 2019. In-season early mapping of rice area and flooding dynamics from optical and SAR satellite data. Eur. J. Remote Sens. 52, 206-220.

Tian, G.X., Li, H.P., Jiang, Q., Qiao, B.J., Li, N., Guo, Z.W., Zhao, J.H., Yang, H.J., 2023. An Automatic Method for Rice Mapping Based on Phenological Features with Sentinel-1 Time-Series Images. Remote Sens. 15, 2785.

Tian, J., Philpot, W.D., 2015. Relationship between surface soil water content, evaporation rate, and water absorption band depths in SWIR reflectance spectra. Remote Sens. Environ. 169, 280-289.

Torbick, N., Salas, W.A., Hagen, S., Xiao, X.M., 2011. Monitoring Rice Agriculture in the Sacramento Valley, USA With Multitemporal PALSAR and MODIS Imagery. IEEE J. Sel. Top. Appl. Earth Obs. Remote Sens. 4, 451-457.

Wang, L.L., Qu, J.J., 2007. NMDI: A normalized multi-band drought index for monitoring soil and vegetation moisture with satellite remote sensing. Geophys. Res. Lett. 34, L20405.

Wang, L.L., Qu, J.J., Hao, X.J., Zhu, Q.P., 2008. Sensitivity studies of the moisture effects on MODIS SWIR reflectance and vegetation water indices. Int. J. Remote Sens. 29, 7065-7075.

Wang, S.L., Li, J.S., Shen, Q., Zhang, B., Zhang, F.F., Lu, Z.Y., 2015. MODIS-Based Radiometric Color Extraction and Classification of Inland Water With the Forel-Ule Scale: A Case Study of Lake Taihu. IEEE J. Sel. Top. Appl. Earth Obs. Remote Sens. 8, 907-918.

Wulder, M.A., Loveland, T.R., Roy, D.P., Crawford, C.J., Masek, J.G., Woodcock, C.E., Allen, R.G., Anderson, M.C., Belward, A.S., Cohen, W.B., Dwyer, J., Erb, A., Gao, F., Griffiths, P., Helder, D., Hermosilla, T., Hipple, J.D., Hostert, P., Hughes, M.J., Huntington, J., Johnson, D.M., Kennedy, R., Kilic, A., Li, Z., Lymburner, L., McCorkel, J., Pahlevan, N., Scambos, T.A., Schaaf, C., Schott, J.R., Sheng, Y., Storey, J., Vermote, E., Vogelmann, J., White, J.C., Wynne, R.H., Zhu, Z., 2019. Current status of Landsat program, science, and applications. Remote Sens. Environ. 225, 127-147.

Xia, T., Ji, W.W., Li, W.D., Zhang, C.R., Wu, W.B., 2021. Phenology-based decision tree classification of rice-crayfish fields from Sentinel-2 imagery in Qianjiang, China. Int. J. Remote Sens. 42, 8124-8144.

Xiao, X., Boles, S., Frolking, S., Li, C., Babu, J.Y., Salas, W., Moore, B., 2006. Mapping paddy rice agriculture in South and Southeast Asia using multi-temporal MODIS images. Remote Sens. Environ. 100, 95-113.

Xiao, X., Boles, S., Frolking, S., Salas, W., Moore, B., Li, C., He, L., Zhao, R., 2002. Observation of flooding and rice transplanting of paddy rice fields at the site to landscape scales in China using VEGETATION sensor data. Int. J. Remote Sens. 23, 3009-3022.

Xiao, X., Boles, S., Liu, J., Zhuang, D., Frolking, S., Li, C., Salas, W., Moore III, B., 2005.

Mapping paddy rice agriculture in southern China using multi-temporal MODIS images. Remote Sens. Environ. 95, 480-492.

Xu, S., Zhu, X., Chen, J., Zhu, X., Duan, M., Qiu, B., Wan, L., Tan, X., Xu, Y.N., Cao, R., 2023. A robust index to extract paddy fields in cloudy regions from SAR time series. Remote Sens. Environ. 285, 113374.

Zhan, P., Zhu, W.Q., Li, N., 2021. An automated rice mapping method based on flooding signals in synthetic aperture radar time series. Remote Sens. Environ. 252, 112112.

Zhan, Z., Qin, Q., Abduwasit, G., Wang, D., 2007. NIR-red spectral space based new method for soil moisture monitoring. Sci. China Ser. D Earth Sci. 50, 283-289.

Zhang, C.K., Zhang, H.Y., Tian, S.J., 2023. Phenology-assisted supervised paddy rice mapping with the Landsat imagery on Google Earth Engine: Experiments in Heilongjiang Province of China from 1990 to 2020. Comput. Electron. Agr. 212, 108105.

Zhang, G., Xiao, X., Dong, J., Kou, W., Jin, C., Qin, Y., Zhou, Y., Wang, J., Menarguez, M.A., Biradar, C., 2015. Mapping paddy rice planting areas through time series analysis of MODIS land surface temperature and vegetation index data. ISPRS J. Photogramm. Remote Sens. 106, 157-171.

Zhang, L., Zhang, L., 2022. Artificial Intelligence for Remote Sensing Data Analysis A Review of Challenges and Opportunities. IEEE Geosci. Remote Sens. Mag. 10, 270-294.

Zhang, W.C., Liu, H.B., Wu, W., Zhan, L.Q., Wei, J., 2020. Mapping Rice Paddy Based on Machine Learning with Sentinel-2 Multi-Temporal Data: Model Comparison and Transferability. Remote Sens. 12, 1620.

Zhang, X., Yang, G., Xu, X., Yao, X., Zheng, H., Zhu, Y., Cao, W., Cheng, T., 2021. An assessment of Planet satellite imagery for county-wide mapping of rice planting areas in Jiangsu Province, China with one-class classification approaches. Int. J. Remote Sens. 42, 7610-7635.

Zhang, Y., Hou, K., Qian, H., Gao, Y., Fang, Y., Xiao, S., Tang, S., Zhang, Q., Qu, W., Ren, W., 2022. Characterization of soil salinization and its driving factors in a typical irrigation area of Northwest China. Sci. Total Environ. 837, 155808.

Zhong, L., Hu, L., Zhou, H., 2019. Deep learning based multi-temporal crop classification. Remote Sens. Environ. 221, 430-443.

Zhou, Y.T., Xiao, X.M., Qin, Y.W., Dong, J.W., Zhang, G.L., Kou, W.L., Jin, C., Wang, J., Li, X.P., 2016. Mapping paddy rice planting area in rice-wetland coexistent areas through analysis of Landsat 8 OLI and MODIS images. Int. J. Appl. Earth Obs. Geoinf. 46, 1-12.